

---

# **Response to Requests for Additional Information for the Review of the ARCADIA<sup>®</sup> Reactor Analysis System for PWRs Methodology Description and Benchmarking Results Topical Report**

ANP-10297Q1NP  
Revision 0

## Topical Report

March 2011

AREVA NP Inc.

---

(c) 2011 AREVA NP Inc.

**Copyright © 2011**

**AREVA NP Inc.  
All Rights Reserved**

### Nature of Changes

Item	Section(s) or Page(s)	Description and Justification
1	All	Original Issue

## Contents

	<u>Page</u>
1.0 INTRODUCTION .....	1-1
2.0 AREVA NP RESPONSES TO RAIS .....	2-2

## **1.0 INTRODUCTION**

The ARCADIA® Topical Report [1-1] was submitted to the US Nuclear Regulatory Commission for review in March 2010. A draft set of Requests for Additional Information (RAI) was released by the NRC in December 2010. This document addresses the AREVA NP Inc. responses to a subset of these RAIs.

### Reference

- 1-1 ANP-10297P, Revision 0, ARCADIA®: Reactor Analysis System for PWRs Methodology Description and Benchmarking

## **2.0 AREVA NP RESPONSES TO RAIS**

This section contains the AREVA NP Inc. Responses to the NRC RAIs. These responses do not address all of the RAIs. The remaining RAIs will be addressed based on a 60 day schedule.

**RAI 1** ARTEMIS uses a single cross section library to span the entire range of application temperatures (hot to cold). Please address the following points on page 1-2:

- The report does not directly address qualification at cold conditions, though most of the critical experiments are at cold conditions.
- No information is provided on how ARCADIA addresses the typical differences between hot and cold cross section libraries.
- Important differences can be the xenon treatment (cold lattice cases are usually run without xenon, while hot cases typically include equilibrium xenon), and the Doppler treatment (cold cases are typically run isothermal, while hot cases typically have independent fuel temperature branches).
- There is also no documented validation of the cold cross section library model to reinforce its applicability during cold transients.

### AREVA Response

*This response for bullet four pertains to cold temperatures not cold transients.*

The cross section libraries are functionalized continuously from hot conditions to cold conditions to handle both temperature changes and the corresponding density changes. The functional dependence of the library against all independent variables (such as xenon and fuel temperature) is available at all temperature conditions. Branch cases are used at a large variety of conditions (including cold states) to determine the functional dependence of the cross sections. The methodology of the cross section tables is described in Section 3.5. ARCADIA utilizes a cross section library structure similar to that employed by CASMO/NEMO [1] and SCIENCE [2] (both previously approved by USNRC).

The underlying cross sections calculated by APOLLO2-A are qualified at cold conditions based on the agreement of APOLLO2-A to measured criticality conditions for critical experiments at cold temperatures. Section 6.2 contains many APOLLO2-A calculations at cold conditions and shows the accuracy of the APOLLO2-A at these temperatures.

### References

1. BAW-10180-A, "NEMO – Nodal Expansion Method Optimized," Revision 1, March,, 1993
2. BAW-10228P-A, "SCIENCE", December, 2000.

**RAI 3** [Page 3-13] The homogenized cross section case matrix used by ARTEMIS appears to be functionalized by only instantaneous perturbations. Spectral (energy) or geometric (shape) corrections induced by depletion at off-nominal conditions have been excluded from the discussion (such as moderator temperature history, fuel temperature history, boron history, and/or control rod history). Is ARCADIA using a pseudo-microscopic model? If so, justification for equation 3-38 should be provided to address omission of multi-dimensional combinatorial effects (i.e. the total homogenized worth in course-group  $g$  is not equivalent to the sum of the worths of the individual isotopes due to the combined effects on the flux spectrum (neutron competition)).

### AREVA Response

The ARTEMIS calculation uses a detailed microscopic cross section model with [ ] explicitly treated isotopes. The microscopic cross sections are functionalized by instantaneous perturbations. From experience with previous code systems, the reactivity effect of depletion at off-nominal conditions is known to be dominated by changes in the nuclide densities. The effect of the change in the microscopic cross sections is generally a secondary minor effect. This was confirmed by running the following calculations.

- A “base” depletion using the APOLLO2-A code. This depletion was performed at typical core average conditions for a reactor at hot full power.
- A “perturbed” depletion using the APOLLO2-A code. The perturbation was induced by an increase in the moderator temperature of 20 K and a corresponding change in the moderator density.
- Branch cases from the “perturbed” depletion in which the moderator temperature was decreased by 20 K along with the corresponding moderator density change. These branch cases are thus run at the instantaneous condition of the “base” depletion.

The differences in reactivity of these cases compared to those of the base depletion are due to the spectral effects of depletion at off-nominal conditions. These cases include changes in the nuclide densities due to the depletion at off-nominal conditions. They also include the effect of the modified nuclide vector on the corresponding microscopic cross sections.

For a typical fuel assembly with 40 GWD/MTU of burnup at the perturbed state, the above calculation yielded a reactivity effect of [ ] .

Then a cross section library was generated for ARTEMIS using the standard methods for this process. The ARTEMIS code was then used to run the same calculations;

- A “base” depletion at nominal conditions.

- A “perturbed” depletion with an increased moderator temperature of 20 K and the corresponding change in the moderator density.
- Branch cases from the “perturbed” depletion in which the moderator temperature was decreased by 20 K along with the corresponding moderator density change. These branch cases are thus run at the instantaneous condition of the “base” depletion.

The differences in reactivity of these cases compared to those of the base depletion are due to the spectral effects of depletion at off-nominal conditions. These cases include changes in the nuclide densities due to the depletion at off-nominal conditions. There are no changes in the microscopic cross sections since the cross section library was used to evaluate these values. For the same fuel assembly used in the APOLLO2-A calculations, the reactivity change due to depletion at the off-nominal conditions was calculated to be [                      ]. Thus, [                      ] of the spectral effect was obtained by the change in the nuclide densities that is treated by the detailed microscopic cross section model used in ARTEMIS.

**RAI 4** On page 3-18, ARTEMIS calculates the fuel rod exposures by integration of fuel rod powers over the nodal depletion.

- Are the fuel rod exposures maintained in the assembly repository throughout the life of the fuel (i.e. is the fuel rod exposures shuffled?).
- Does this also mean that the fuel rod exposures calculated by APOLLO2-A are essentially ignored?

#### **AREVA Response**

The fuel rod exposures are maintained in the assembly repository throughout the life of the fuel. These values include each axial level used in the core model. The fuel rod information is updated to reflect any assembly rotation during the shuffling process. The fuel rod exposures calculated by APOLLO2-A are essentially ignored.

**RAI 5** On page 3-19, ARTEMIS uses the infinite lattice detector flux form factor to calculate the neutron detector reaction rate in the instrument tube. This assumes that the reconstructed flux is relatively equal to the infinite lattice flux, for the regions near the instrument tube. Is this assumption also valid for peripheral fuel assemblies?

### **AREVA Response**

The detector flux form factor provides the ratio of the heterogeneous detector flux to the homogeneous flux at the detector location. The assumption is that the reconstructed homogeneous flux is accurately determined at the detector location. The group-wise homogeneous flux at the detector location is determined using the two dimensional flux within each node as determined by the dehomogenization (reconstruction) process. The flux is integrated over the corresponding local region (cell) that contains the detector. This takes into account the flux gradients that occur in peripheral fuel assemblies. The flux is then multiplied by the detector flux form factor to provide the heterogeneous group-wise flux in the detector.

**RAI 10** On page 4-2, the ARTEMIS/COBRA-FLX coupling accounts for cross flow effects. Have these effects been evaluated for PWR conditions undergoing two-phase flow (accident scenario)?

### AREVA Response

It is recognized that the quoted statement in Ref. [1] implies unintended data flow from the COBRA-FLX module to the rest of the ARCADIA package due to the use of the word “main” in the text, which is not further clarified in this section.

As stated on pg. 4-5 in Ref. [1], COBRA-FLX coupling with ARTEMIS is twofold.

- a. Generating the required information for the cross-section updates during the flux iteration process, and
- b. Thermal-hydraulic evaluation of the power density distribution resulting from a converged flux solution.

The data passed back to ARTEMIS from COBRA-FLX for the purpose of cross section updates (during the flux iteration process) are: node-average coolant temperatures, coolant densities, and void fractions [1, pp. 4-6, 3-21]. In order to calculate these coolant properties, COBRA-FLX obtains the data pertaining to the core power distribution from ARTEMIS [1, pp. 4-6]. Therefore, the calculations and the use of cross flows for determining the nodal coolant conditions are contained within the COBRA-FLX module, which in turn calculates the node specific coolant properties to be passed onto ARTEMIS.

Examples of COBRA-FLX Transient (accident) simulations involving two phase flow are provided in Section 5.7.2 in Ref. [2]. Section 5.5 in Ref. [2] provides comparisons of COBRA-FLX modeling the 4 pump coast down transient with varying model complexity that ranges from 12 channels where lumped channels are involved, to 7083 channels where all subchannels are individually modeled. Results provided in Table 5-6 in Ref. [2] show excellent agreement between varying degrees of modeling detail.

### References

1. ANP-10297P, Rev 0, The ARCADIA® Reactor Analysis System for PWRs Methodology Description and Benchmarking Results, March 2010.
2. ANP-10311P, Rev 0, COBRA-FLX: A Core Thermal-Hydraulic Analysis Code Topical Report, March 2010.

**RAI 11** On page 5-1, 5- 5, the ARTEMIS Fuel Rod Methodology (FRM) solves the one-dimensional heat conduction equations (static and time-dependent) for the average fuel rod in each node. The effective temperature is calculated for nodal cross section evaluation using equation 5-2, which is NOT a simple volume-average (VAFT). Please provide qualitative and quantitative technical Justification for this equation

### AREVA Response

The effective temperature evaluation as shown in equation 5-2 is the same as the equation used in ANP-10286P [1] (end of section 6.2.4) and in ANP-2788P [2] (end of section 6.2.4).

In a qualitative sense, [

]

The relationship for the effective temperature ( $T_{\text{eff}}$ ) has been validated with the computer code APOLLO2 described in BAW-10228PA, (Reference 3). The reactivity and U-238 capture rate of several snapshot fuel temperature distributions at steady state conditions and those temperatures expected during a Reactivity Initiated Accident (RIA) event were examined with APOLLO2. Calculations were repeated with a uniform fuel temperature until the reactivity and U-238 capture rates were equivalent to the nonuniform temperature distributions. This uniform temperature was defined as the effective temperature and compared to the values predicted by Rowland's formula and the new  $T_{\text{eff}}$  formula. Fifteen cases were run for each temperature distribution, which spanned burnups from 0 to 60 GWD/MTU and U-235 enrichments from [ ] weight percent (w/o). Results showed that Rowland's formula resulted in nearly the same temperature as the new  $T_{\text{eff}}$  formula for steady state cases, and that both agreed with the APOLLO2 effective temperature. For the transient fuel temperature cases, the new  $T_{\text{eff}}$  definition showed substantial improvement reducing the mean prediction error of  $T_{\text{eff}}$  from a range [ ] K for the Rowland's formula down to a range of [ ] K. Both models had about a [ ] K standard deviation. The APOLLO2 temperature solution was benchmarked to Monte Carlo N-Particle (MCNP) transport code calculations. In addition, the new  $T_{\text{eff}}$  method was compared in Table 7-5 of Reference 2 to an average temperature formulation and was found to yield slightly more limiting results than a simple average weighting.

### References

1. ANP-10286P, Revision 0, "U.S. EPR Rod Ejection Accident Methodology Topical Report," November 2007, AREVA NP, Inc.
2. ANP-2788P, Revision 0, "Crystal River 3 Rod Ejection Accident Methodology Report", February 2009, AREVA NP, Inc.

---

3. BAW-10228P-A, "SCIENCE", December, 2000.

**RAI 21** Section 7.3.1 states that “Generally, the cross-sections for the ARTEMIS reflector model are transformed into microscopic cross sections.” Please explain under which conditions this transformation is done and why? Please clarify which model is used for the benchmarks [Page 7-3].

**AREVA Response**

The microscopic representation of the reflector cross sections is the standard model. All calculations in the Topical Report were performed using the standard model. The macroscopic model is available in ARTEMIS for internal comparisons with other AREVA codes. It is not AREVA’s intent to use the macroscopic reflector cross section representation.

The advantage of the microscopic representation is a more explicit treatment of the non-linearity of the moderator density.

**RAI 22** For “heavy reflectors”, (reflectors comprised of a thick steel shroud and low moderation inside the core barrel), the water scattering cross sections are calibrated with factors “deduced from the comparison of the 2D power density distribution calculated by ARTEMIS with the corresponding reference MCNP result”. The methodology used to “deduce” these factors should be documented and some justification should be made as to the application of the modified scattering cross section to other plant/fuel types. A quantification of the magnitude of the calibration should also be provided. [Page 7-4]

### AREVA Response

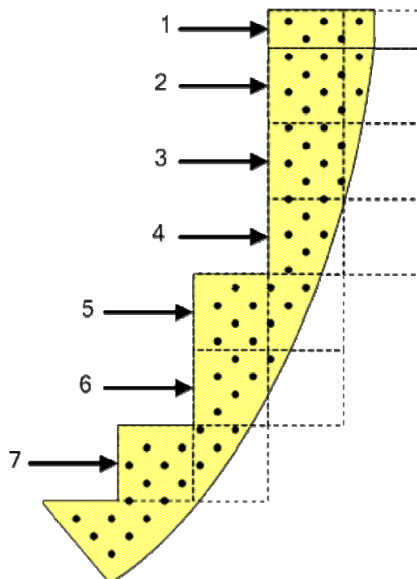
The 1D spectral geometries with reflective boundary conditions used for deriving the cross sections for the radial reflector neglect transverse leakage (2D) effects. For the heavy reflector this leads to discrepancies between ARTEMIS and MCNP reactor calculations when using non-adapted reflector cross sections.

An iterative procedure, a variant of the simulated annealing algorithm, was developed for the purpose of deriving adaptation factors for the heavy reflector cross sections. The procedure adapts the microscopic slowing-down cross section of H<sub>2</sub>O until spread and standard deviation of the differences of the normalized core wide power density distribution of ARTEMIS and the fission rate distribution of MCNP are minimized. In ARTEMIS the normalized power density and fission rate distribution is consistent.

Two types of adaptation factors were found to be sufficient for avoiding heavy reflector induced in/out or azimuthal trends, one for non in-side (edge) and one for re-entrant (corner) reflector nodes. The classification of the heavy reflector nodes is (see Figure 7.3-2 of the Topical Report):

reflector nodes 1, 2, 3, 4, 6 → edge  
reflector nodes 5, 7 → corner

Figure 7.3-2: Heavy Reflector Geometry



**Copy of Topical Report Figure  
7.3-2**

---

The resulting adaptation factors are 3.02 for the edge reflector nodes and 4.01 for the corner reflector nodes.

The qualification of the derived heavy reflector cross sections is shown in Figure 7.3-3 of the Topical Report. For this qualification a significant number of core calculations with varying state parameters (variation of boron concentration and moderator temperature) were calculated with ARTEMIS and MCNP and the results compared. In addition these reflector cross sections were applied to an independent core loading pattern. As can be seen in the figure there is no dependence of the spread and the standard deviation on these parameters. The deviations are of the same size as for the cases with standard shroud/water reflector. The variation of the deviations is in the order of magnitude of the Monte Carlo calculation.

**RAI 23** The report states that, regarding power distribution comparison against MCNP, “no in/out or azimuthal trends of the error distribution can be identified”. However, both Figures 7.3-4 and 7.3-5 display clear trends with distance from the reflector (in/out). In both cases, ARTEMIS under-predicts all peripheral assemblies (those next to reflector) and over-predicts most of the assemblies within 2-4 assemblies from the reflector. Furthermore, the case of the heavy reflector significantly under-predicts the power in the center of the core. A very clear radial pattern exists in both figures. [Page 7-6]

### AREVA Response

In the view of comparing results from two independent code systems with very different geometry and energy group representation of the reactor problem the agreement demonstrated in Figures 7.3-4 and 7.3-5 is quite satisfactory. The radial reflector determines the core wide in-out tilt of the fast flux and the very local flux shape at the core/reflector interface by the reflection of thermal neutrons. The representation of the radial reflector is not responsible for deviations in individual fuel assembly types or local core regions as long as the differences of the power densities in the core center and at the core periphery are of the same order of magnitude and of the same direction (negative in these cases).

For both sample problems no significant azimuthal variation of the differences can be observed. This confirms the applicability of the corrections for the re-entrant reflector corners for either a “normal” steel/shroud or a heavy reflector as described in the Topical Report.

**RAI 24** Figures 7.3-4 and 7.3-5 look like full core but the documentation states that MCNP was run with octant symmetry. Why are full core results provided?  
[Page 7-5]

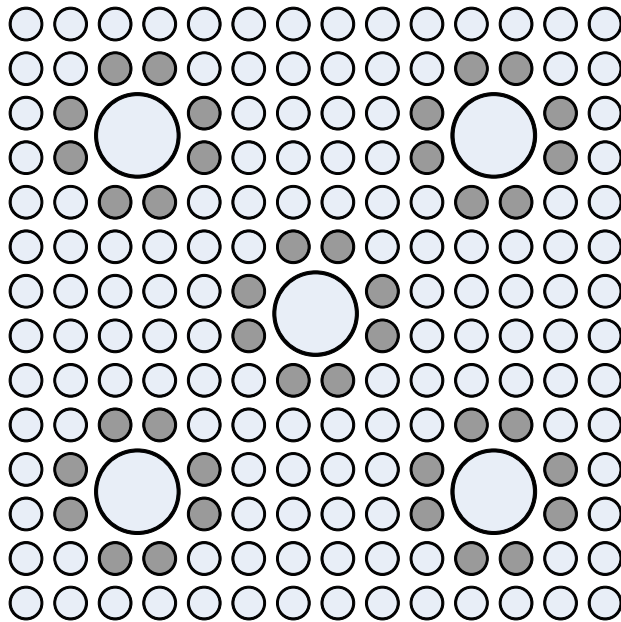
**AREVA Response**

The represented cores are octant symmetric. Nevertheless, the ARTEMIS Calculations were performed in full core geometry. For direct application of existing scripts the MCNP results were unfolded to full core geometry.

**RAI 25** The descriptor “zone-loaded” is used frequently in the benchmarking results section of the report. This term should be defined in the document, possibly with an example image of what it means in terms of lattice enrichment. [Page 10-9]

**AREVA Response**

Zone loading of fuel pins is common in CE type assemblies. The zone loaded fuel pins are pins with a lower enrichment that are inserted adjacent to the guide tubes and the instrument tube to reduce power peaking in these locations. A typical zone loaded assembly lattice is shown below:



Rod Type	# of Rods	Rod Description
	136	High Enriched
	40	Low Enriched

**RAI 26** For startup physics test results, the “measured data has been adjusted to reflect the ARCADIA delayed neutron parameters”. This adjustment should be provided in more detail and some quantification or magnitude should be provided in order to assess the impact on the calculation uncertainty. [Page 10-30]

**AREVA Response**

Plant measurements are made using a reactivity computer where a calculated set of delayed neutron factors and prompt neutron lifetimes are input. These parameters vary based on the reference data used and the process used to generate these parameters. To compensate for this, an approximation is used to adjust the measured data to be consistent with the ARTEMIS generated delayed neutron fractions and prompt neutron lifetimes. This correction is determined as the ratio of the effective delayed neutron fraction from ARTEMIS ( $\beta_{eff\ ARTEMIS}$ ) to the effective delayed neutron fraction from the measurement ( $\beta_{eff\ meas}$ ). The adjustment is made as

$$\beta_{eff\ adjustment} = \frac{\beta_{eff\ Artemis}}{\beta_{eff\ meas}}$$

The  $\beta_{eff}$  adjustments for Plants A, C, S1 and S2 are provided in the following table to illustrate the typical range for this adjustment.

Cycle	$\beta_{eff}$ adjustment			
	Plant A	Plant C	Plant S1	Plant S2
1				
2				
3				
4				
5				
6				
7				
8				
9				
10				
11				
12				
13				
14				
15				
16				
17				
18				

**RAI 27** The exclusion of Bank D from the startup physics summary for Plant A Cycle 11 is not justified. The fact that the bank met the criterion in previous and subsequent cycles does not prove a measurement anomaly, especially without a detailed analysis of other plant differences (core design, flow conditions, rod shadow, etc). Data should not be manipulated to support the desired conclusions. [Page 10-30 ]

**AREVA Response**

The referenced paragraph did not provide enough detail in what the context of “not considered” means. The current pass/fail criterion of 15% or 100 pcm are review criteria for the plant during startup and is being used as a screening criterion for ARCADIA. If all values are less than 15%, then the plant cycles would have passed the startup criteria using ARCADIA. With this screening criterion, one measurement was found that exceeded this criterion with ARCADIA. So the failure rate by ARCADIA for single bank worth comparisons leads to a failure rate of 0.4%. This level of failure rate is reasonably expected. In addition, if we calculate a 95/95 limit for single bank worths for all the plants, it would lead to an uncertainty of less than 15% (see table 27-1). Hence, the ARCADIA prediction for bank D in Plant A Cycle 11 is not considered a failure of ARCADIA. This worth is included in the calculation of total worth.

**Table 27-1, Statistics for Single Bank Worths**

<b>Individual Bank Worth</b>	<b>Mean (%)</b>	<b>Standard Deviation (%)</b>	<b>K factor 265 pts</b>	<b>95/95 Tolerance limit</b>
<b>All plants and cycles</b>	[			] <15% criterion

**RAI 28** Plant G1 Cycle's 27 and 28 had a BOC B10 abundance of 19.2%. Also, Cycle's 29 and 30 used enriched B10 at about 30%. The report states that the Cycle 26 HZP boron measurement "may be suspect because of the B10 isotopic abundance was not measured". However, there are no unexpected comparisons at BOC HFP, which indicates that no additional B10 correction should be necessary at HZP. The report does not clearly describe which boron measurements are adjusted for B-10 content, and which are not. B10 corrections, both at HZP and HFP (i.e. B-10 depletion, if included) should be applied consistently for all cycles and should be clearly documented. [Page 10-31,1035]

### AREVA Response

For Cycle 26 of plant G1 the B-10 abundance was not measured, but the measured B-10 abundances are known for Cycles 27 to 30. These abundances are provided below:

Cycle	B-10 Abundance (a/o B-10)
27	19.20
28	19.25
29	31.61
30	31.55

The measured B-10 abundances from Cycles 27 to 30 were used to adjust the respective measured boron concentrations such that they are relative to natural boron.

For Cycle 26, where no measured B-10 abundance is available, an assumed boron abundance of 19.2 a/o B-10 (Cycle 27 value) is used.

Erroneously the critical boron adjustment in Table G1 10.3.4-1 and in Figure G1 10.4.4-1 of the Topical Report for Cycle 26 was applied to the calculated values to make them relative to the measured B-10 abundance instead of using the assumed measured B-10 abundance to adjust the measured critical boron concentrations such that they are relative to concentrations with natural boron. The values have been updated and are presented in Table 28-G1-1 and Figure 28-G1-1 (see below).

Moreover, in the Tables and Figures of Appendices G1 and G2 an inconsistency in the results has been corrected. The B-10 abundance of natural boron was assumed to be 19.74 a/o when adjusting the measured values, whereas ARTEMIS uses the value 19.9 a/o. To compare boron concentrations directly it is necessary that the adjusted measured boron concentrations correspond to the ARTEMIS B-10 abundance, so in the following tables and figures the measured boron concentrations have been adjusted to correspond to a B-10 abundance of 19.9 a/o.

These corrections have been applied and are shown in Table 28-G1-1, Table 28-G2-1, Figures 28-G1-1 through 28-G1-5 and Figures 28-G2-1 through 28-G2-5.

Plant/Cycle	Measured (ppm)	Calculated (ppm)	Difference C-M (ppm)
G1 Cycle 26	1628	1596	-32
G1 Cycle 27	1764	1757	-7
G1 Cycle 28	1638	1593	-45
G1 Cycle 29	1689	1648	-41
G1 Cycle 30	1760	1716	-44

Table 28-G1-1: Plant G1 Hot Zero Power All Rods Out Critical Boron Concentrations for Cycles 26-30

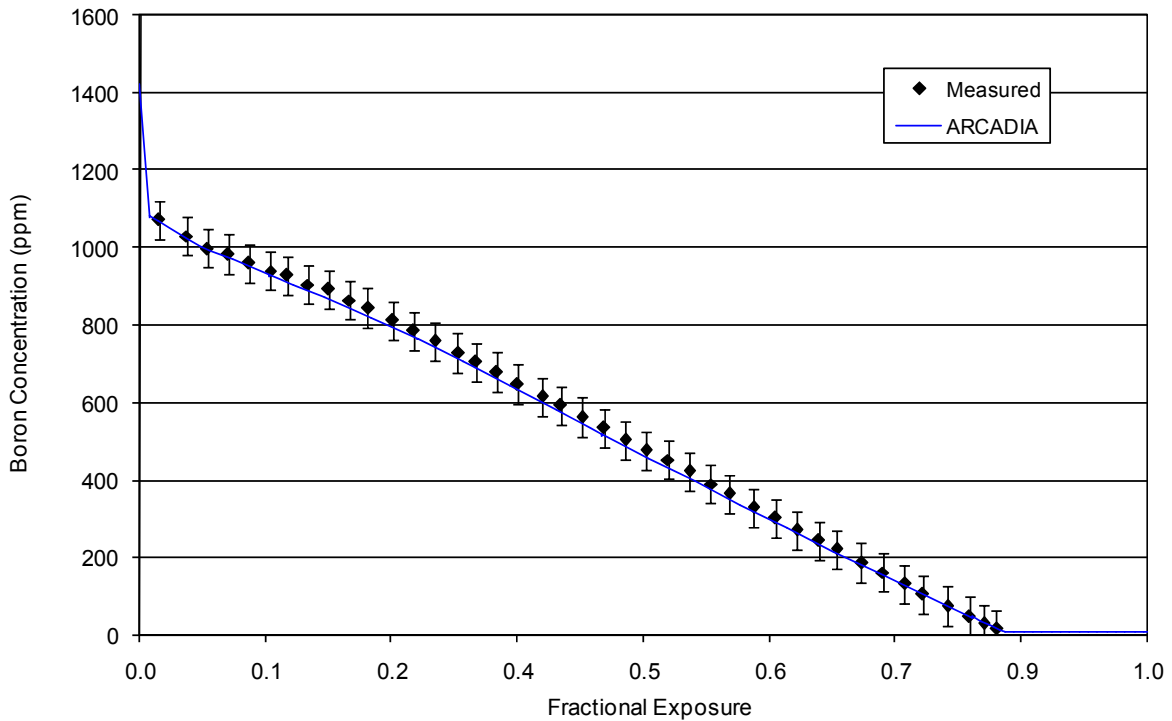


Figure 28-G1-1: Plant G1 Cycle 26 Critical Boron Concentration vs. Burnup

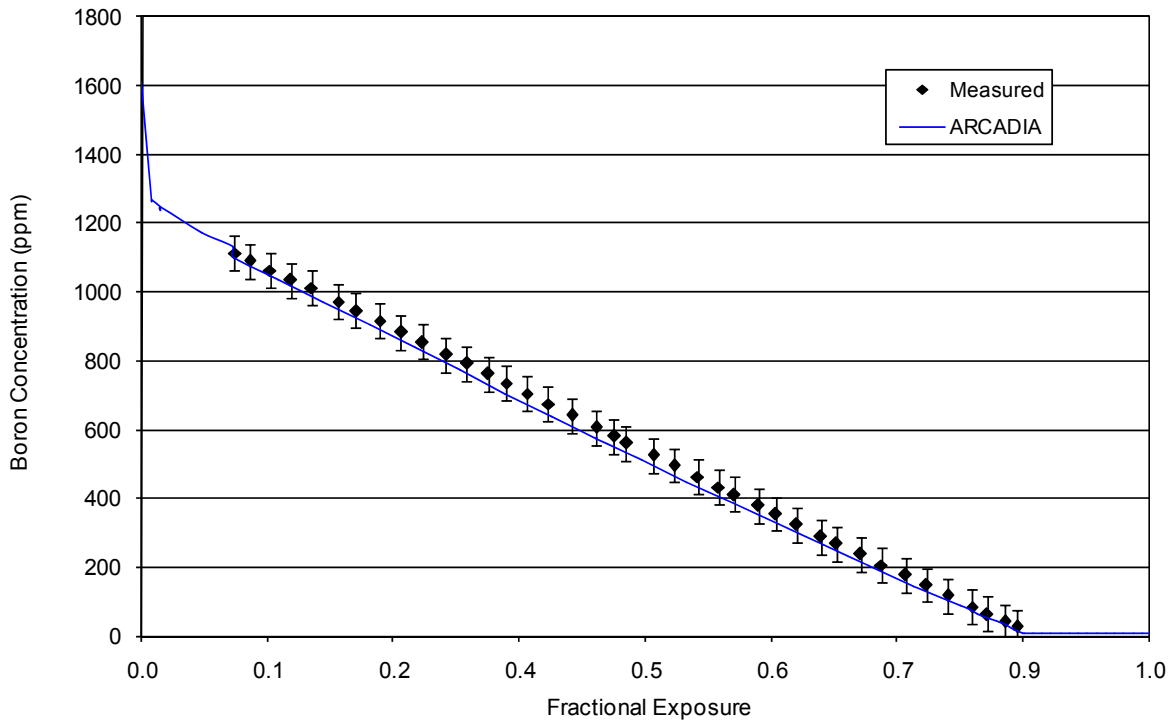


Figure 28-G1-2: Plant G1 Cycle 27 Critical Boron Concentration vs. Burnup

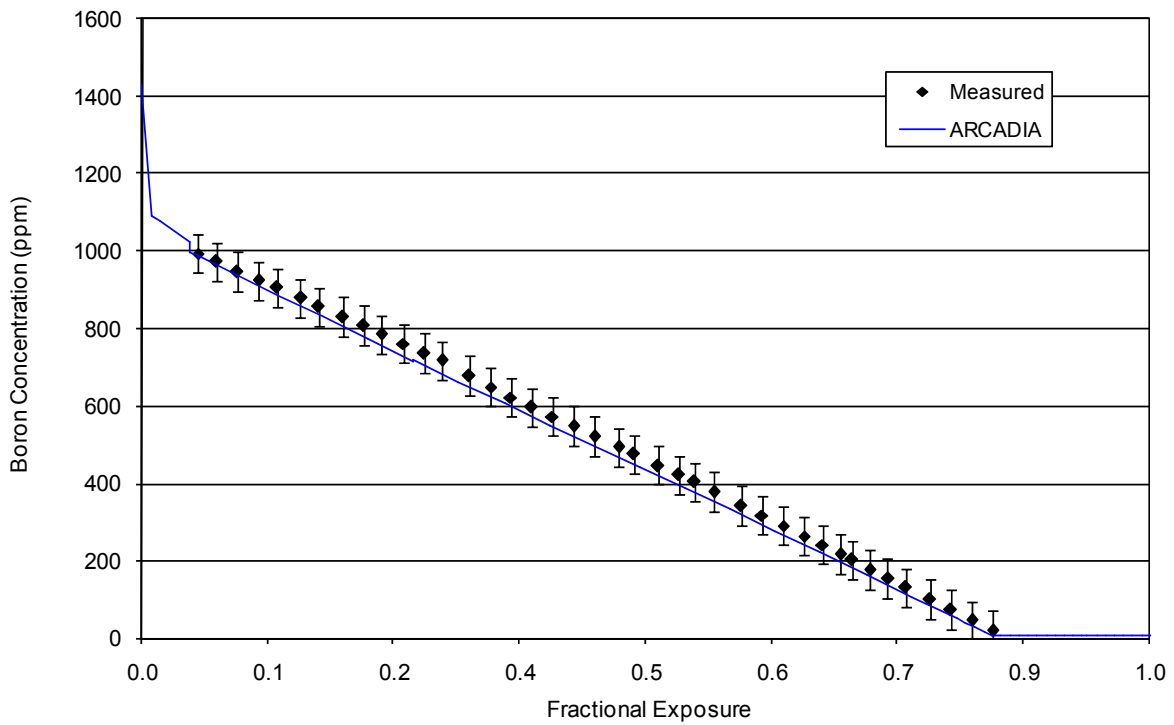


Figure 28-G1-3: Plant G1 Cycle 28 Critical Boron Concentration vs. Burnup

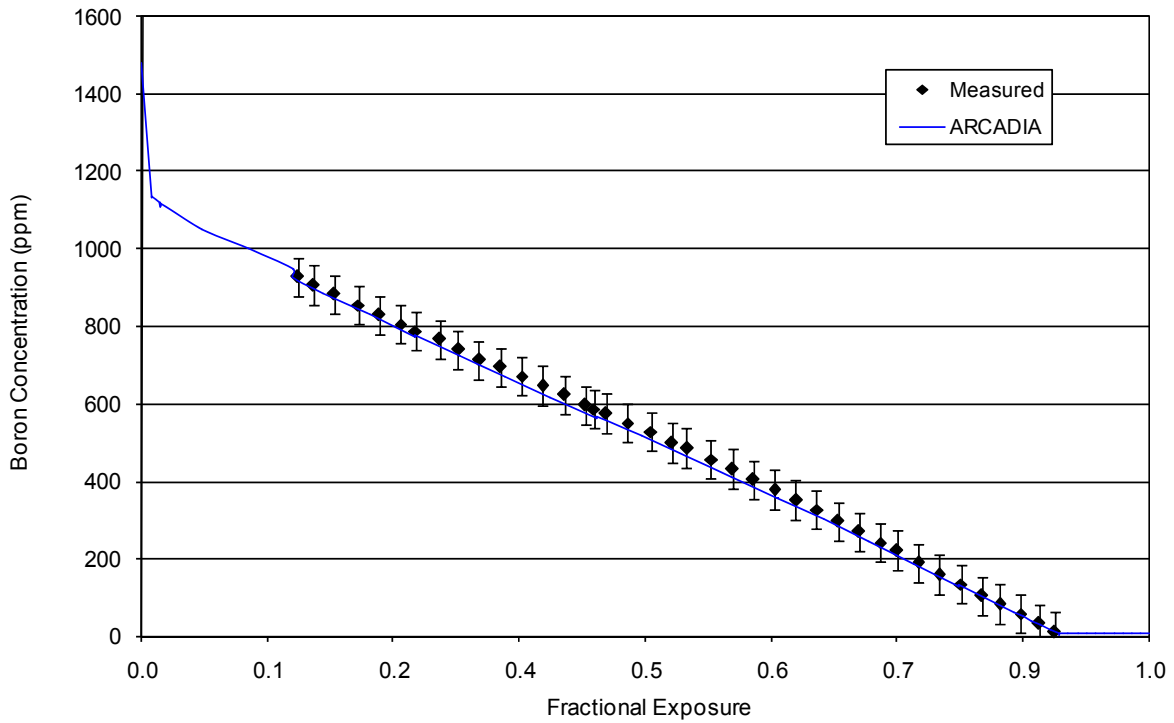


Figure 28-G1-4: Plant G1 Cycle 29 Critical Boron Concentration vs. Burnup

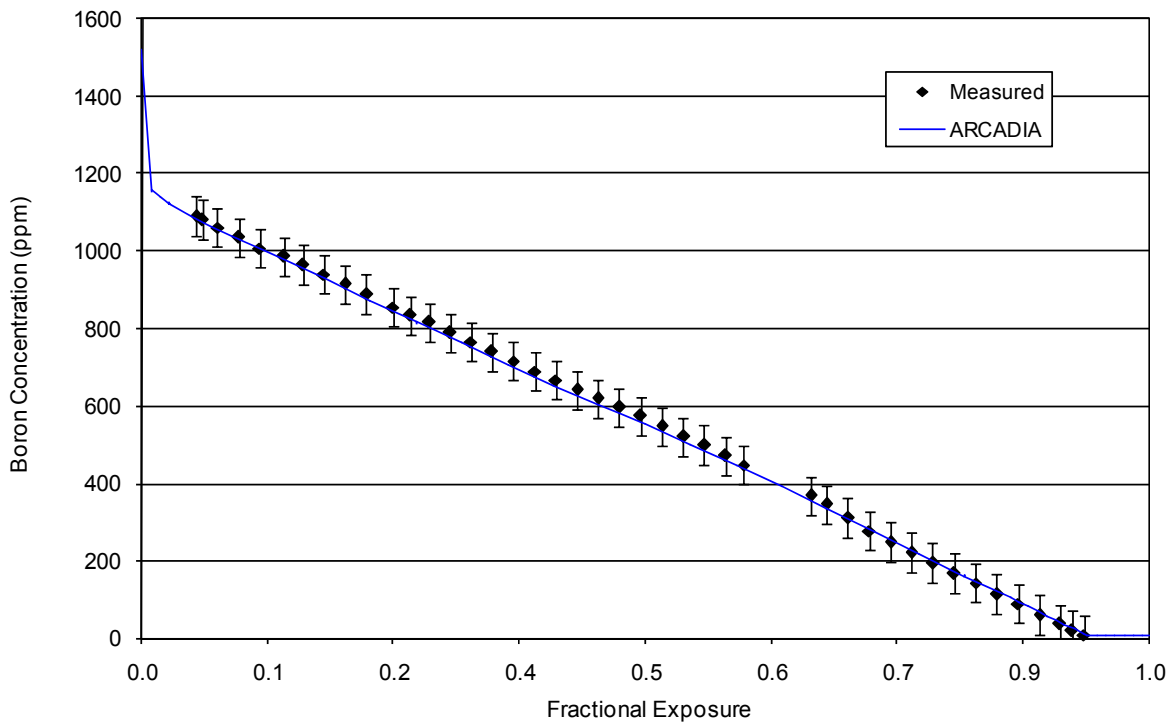


Figure 28-G1-5: Plant G1 Cycle 30 Critical Boron Concentration vs. Burnup

Plant/Cycle	Measured (ppm)	Calculated (ppm)	Difference C-M (ppm)
G2 Cycle 1	1426	1445	19
G2 Cycle 2	1407	1383	-24
G2 Cycle 3	1543	1520	-23
G2 Cycle 4	1396	1381	-15
G2 Cycle 5	1528	1499	-29

Table 28-G2-1: Plant G2 Hot Zero Power All Rods Out Critical Boron Concentrations for Cycles 1-5

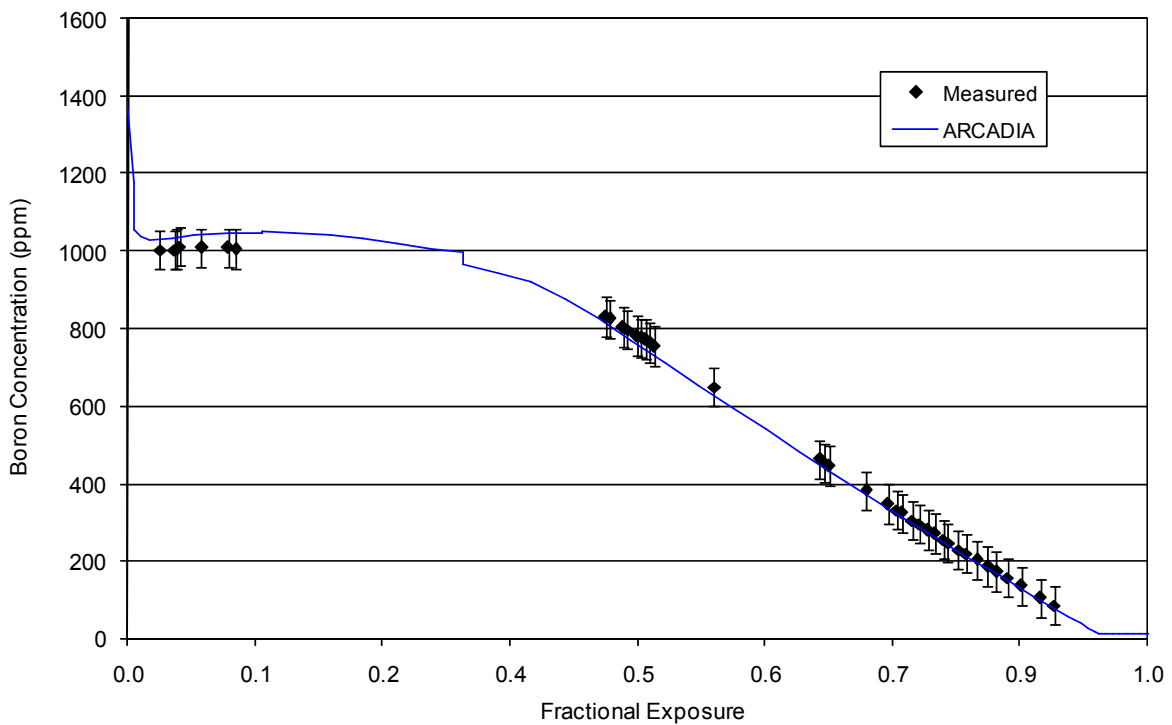


Figure 28-G2-1: Plant G2 Cycle 1 Critical Boron Concentration vs. Burnup

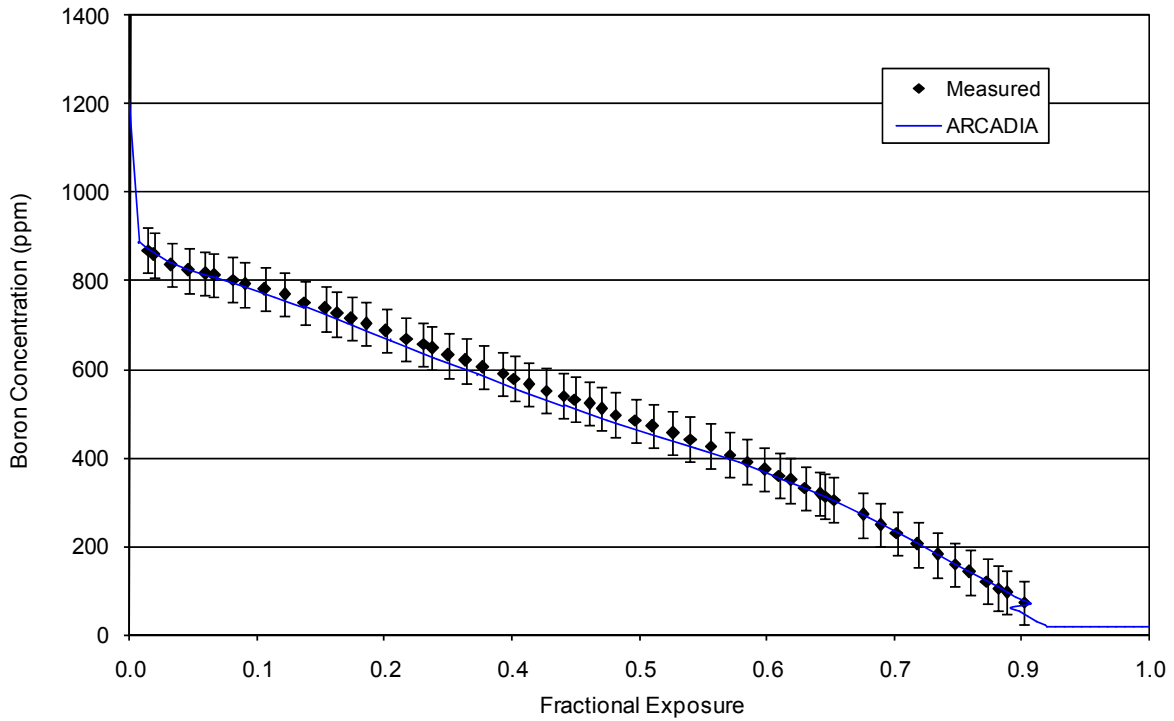


Figure 28-G2-2: Plant G2 Cycle 2 Critical Boron Concentration vs. Burnup

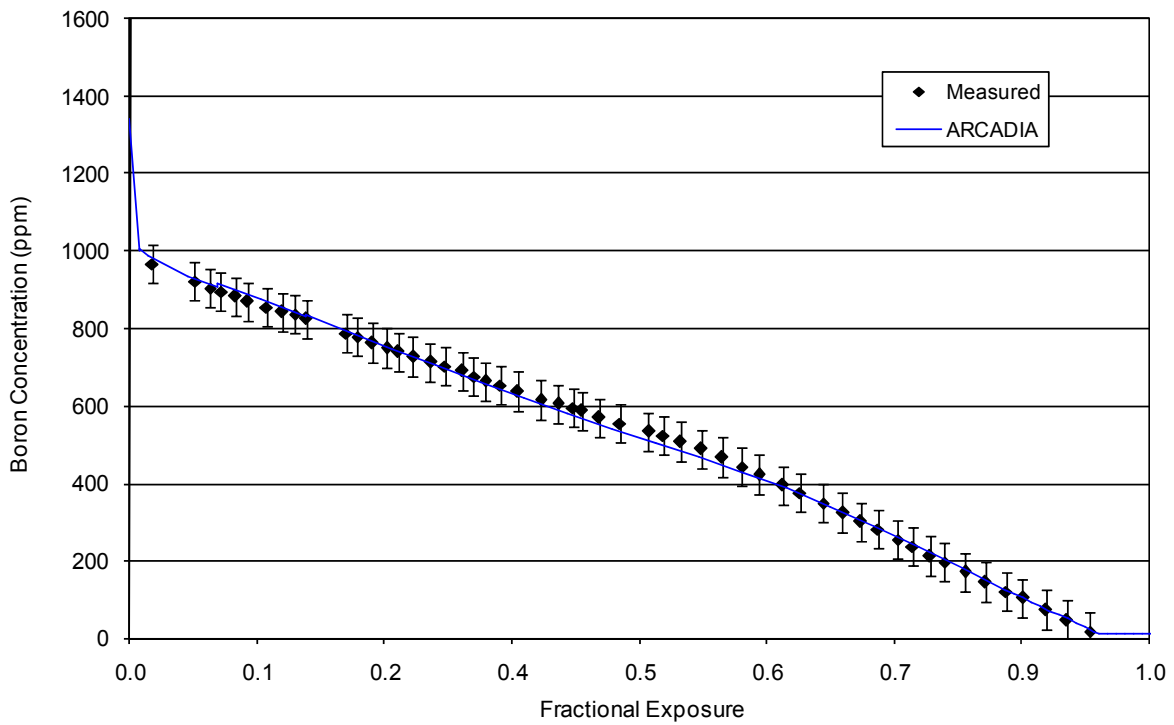


Figure 28-G2-3: Plant G2 Cycle 3 Critical Boron Concentration vs. Burnup

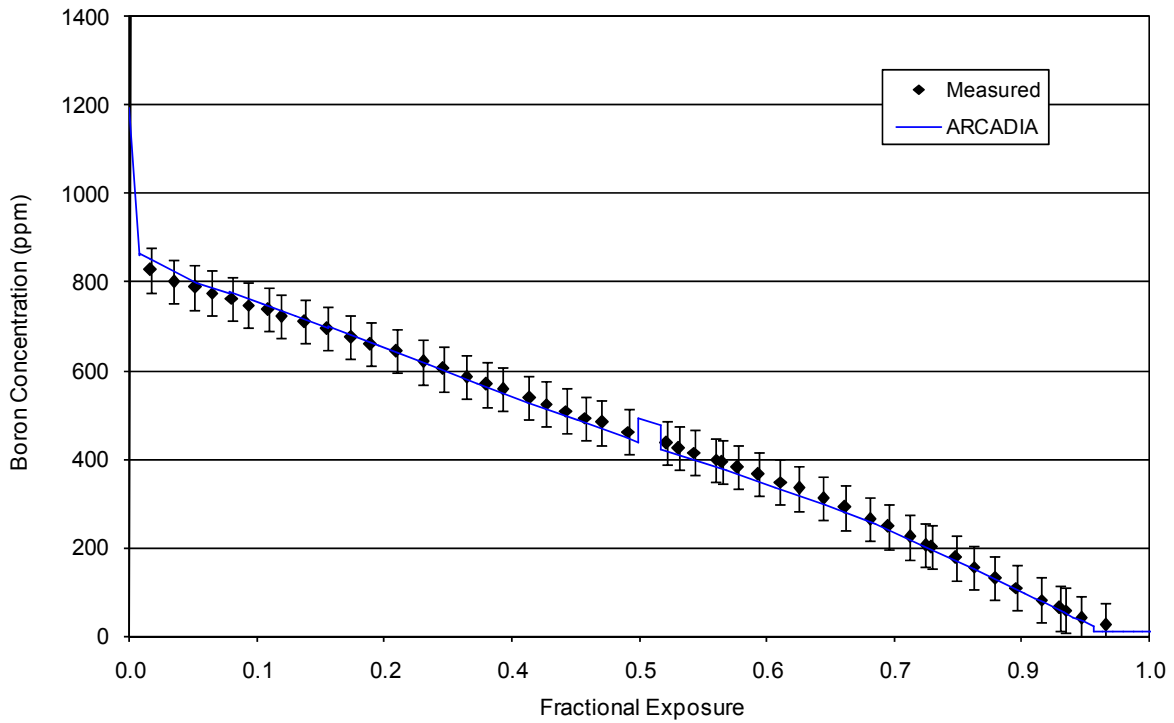


Figure 28-G2-4: Plant G2 Cycle 4 Critical Boron Concentration vs. Burnup

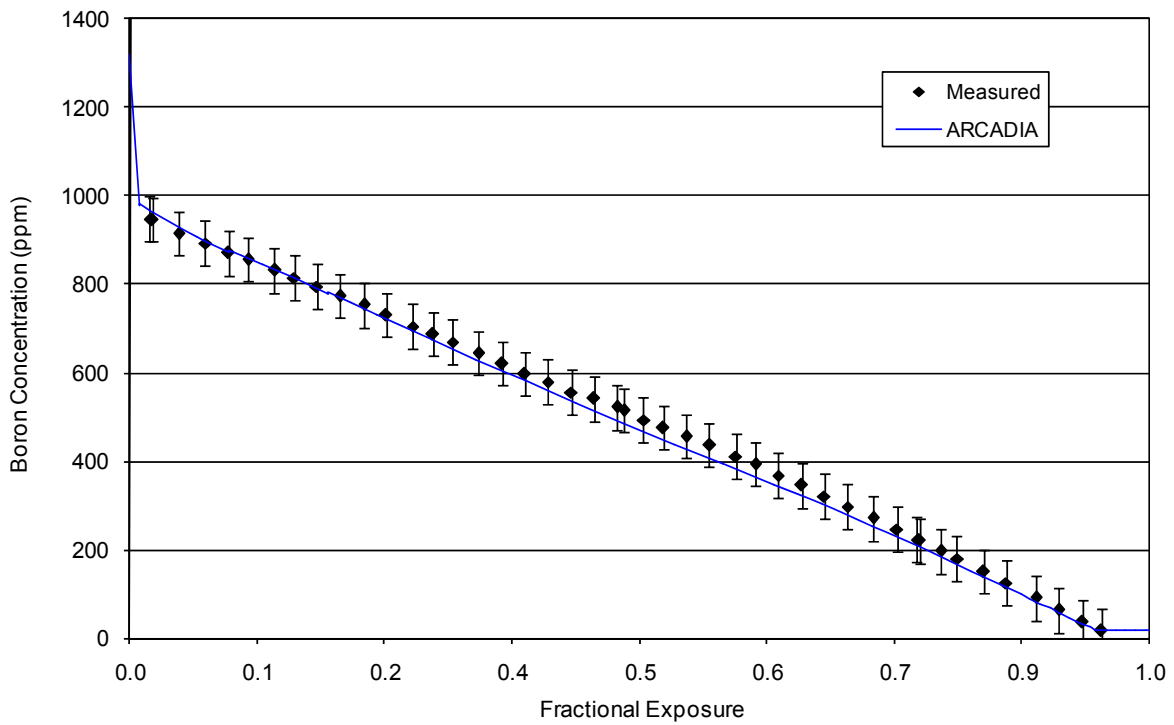


Figure 28-G2-5: Plant G2 Cycle 5 Critical Boron Concentration vs. Burnup

**RAI 29** The reference to 9 cycles cannot be located. Is this intended to be nine cycles per plant (for a typical licensee/operator)? This may have been removed in the latest version of the referenced ANSI/ANS standard. [Page 10-32]

### AREVA Response

A review of the ANSI/ANS-19.6.1-2005 standard does not specify a requirement for a specific number of cycles to be considered. Supplying a reference for this criterion was unintentional. Also Reference 10.6-2 should have specified the 2005 standard (Reference 1) and not the 1995 standard. Reference 10.6-2 will be corrected in the approved version of the ARCADIA® topical report. It is proposed that the wording of the paragraph in question be changed as follows:

*Core follow comparisons include two different plant/fuel types with additional data, as available from Siemens type reactors. A minimum of nine cycles of operation should be considered with at least three cycles of operations per plant type. Core follow predictions are compared to the available data measured at, or near, hot full power for each cycle of each plant/fuel type. The parameters compared are... .*

### Reference

1. Reload Startup Physics Tests for Pressurized Water Reactors, ANSI/ANS-19.6.1-2005, American Nuclear Society, 2005.

**RAI 31** The boron letdown curves are presented for each cycle individually as a function of fractional cycle length. This scale is confusing because it prevents some comparisons from cycle to cycle, and inhibits the ability to approximate cycle length-based effects, such as gadolinia depletion, B-10 depletion, and design implications for 24 vs 12 month cycles, etc. Furthermore, the letdown curves are presented on an absolute value scale, which makes individual deviations very hard to discern. A summary plot of boron difference for all cycles (to compare against each other, potential by plant), plotted versus a non-relative scale such as cycle exposure would be useful. [Page A-9+]

**AREVA Response**

Summary plots of the boron deviations are provided. These plots use an absolute scale for burnup and present the boron deltas for all cycles by plant.

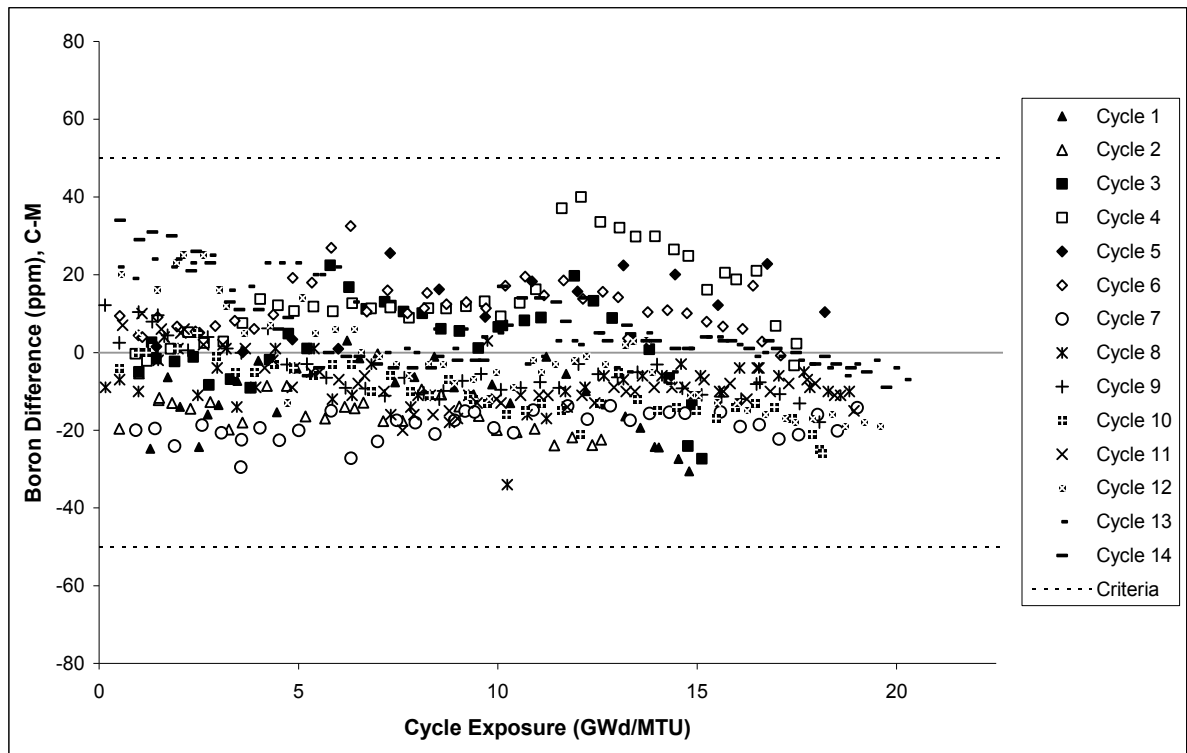


**Figure 31-A-1: Boron Differences**

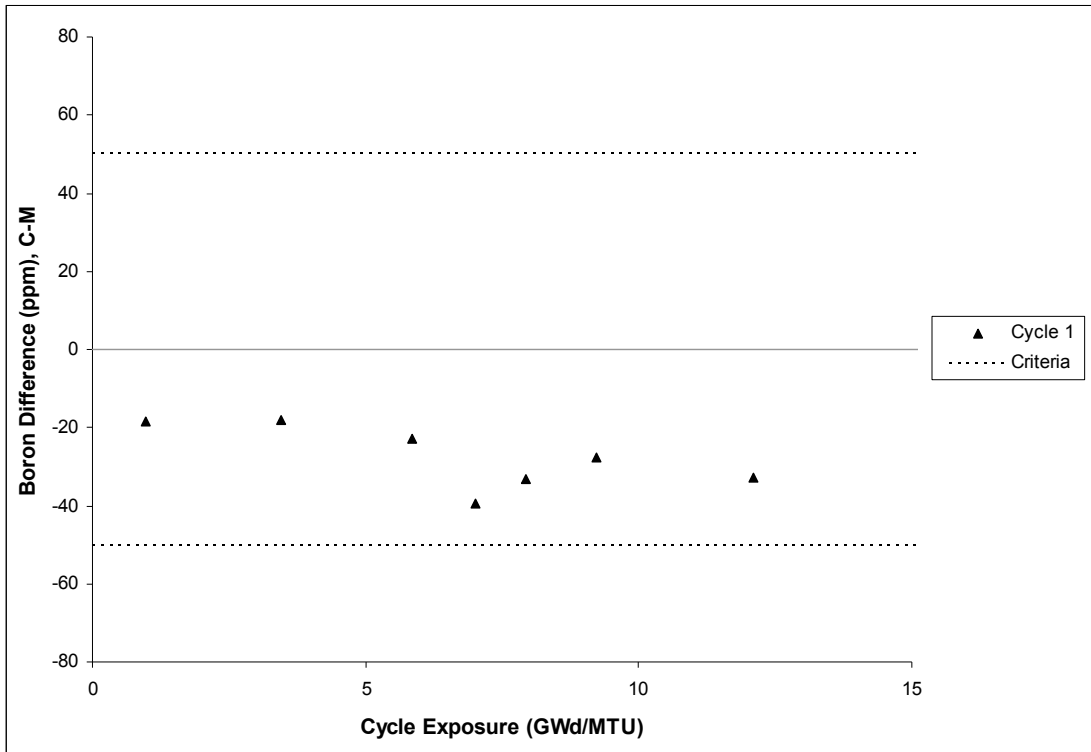


Figure 31-B-1: Boron Differences

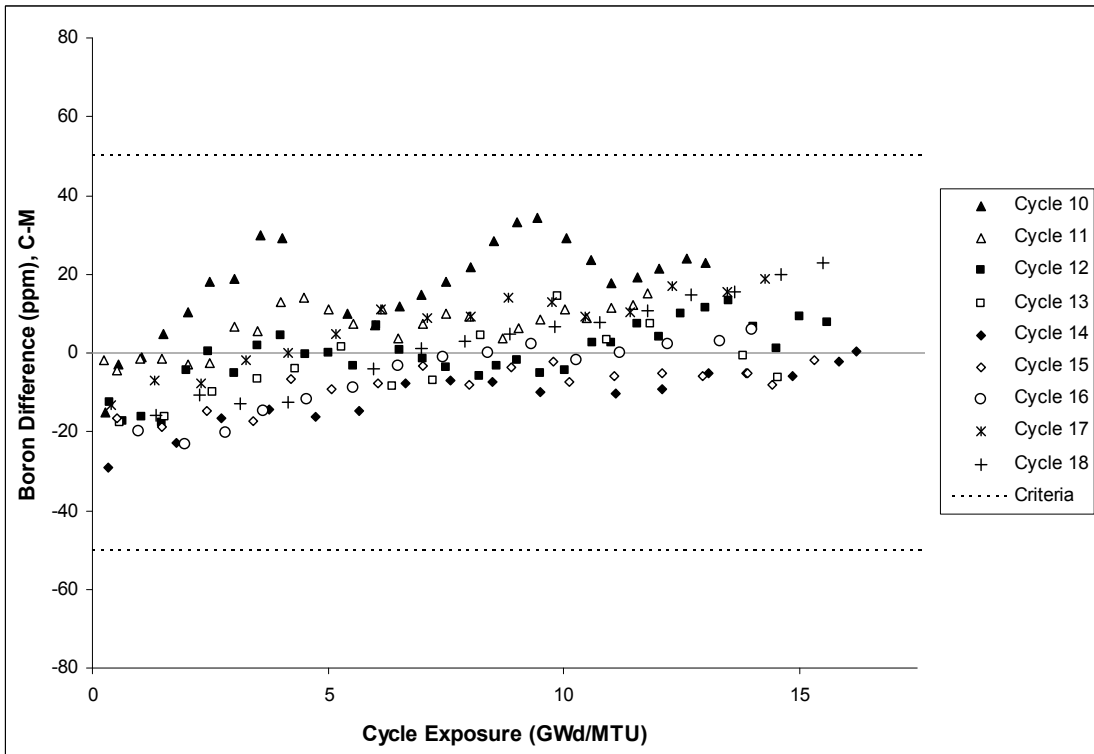


Figure 31-C-1: Boron Differences

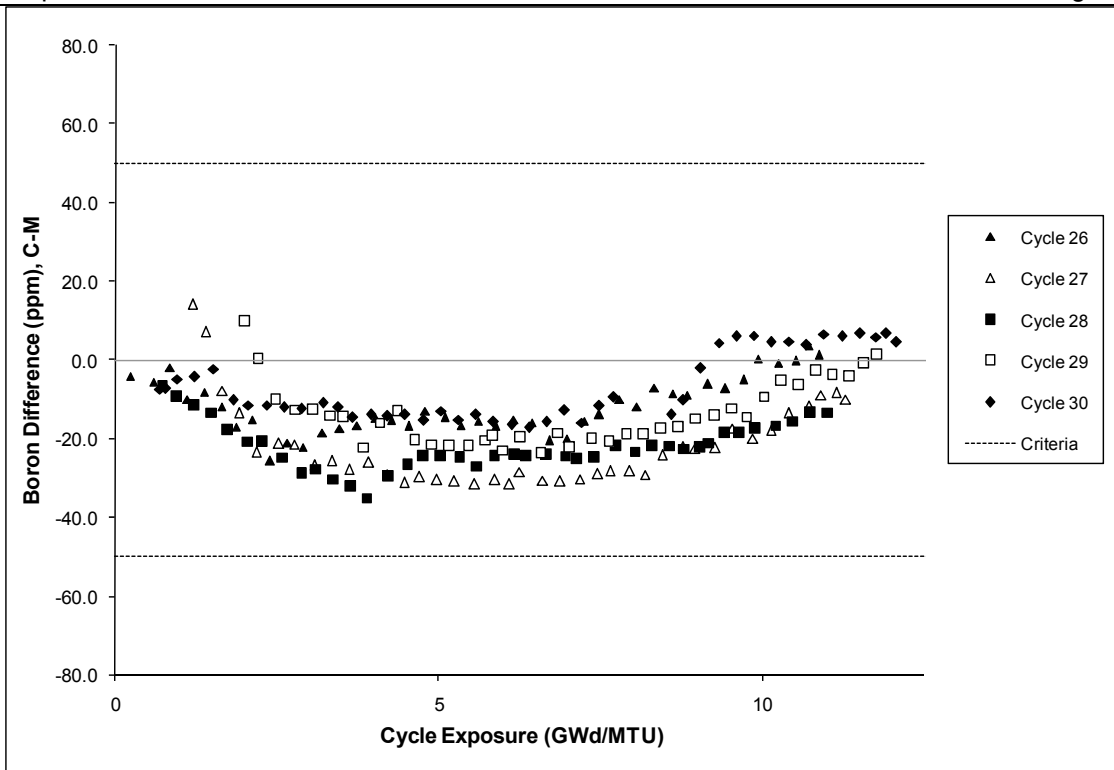


Figure 31-G1-1: Boron Differences

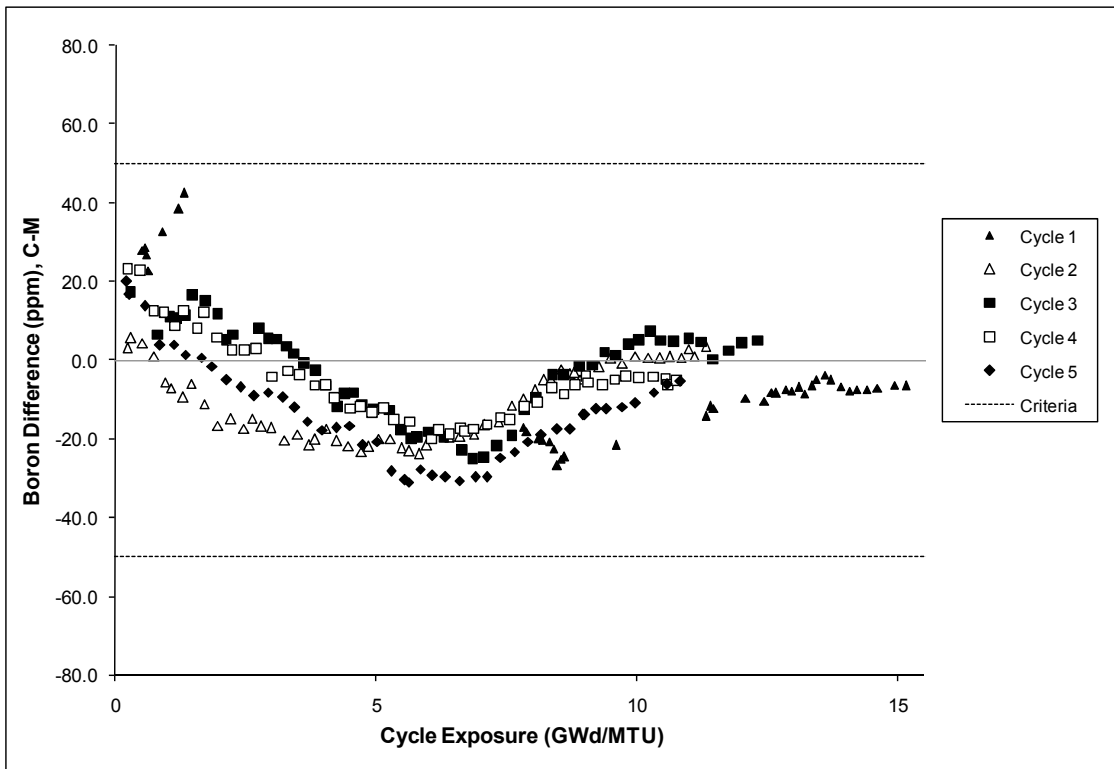


Figure 31-G2-1: Boron Differences

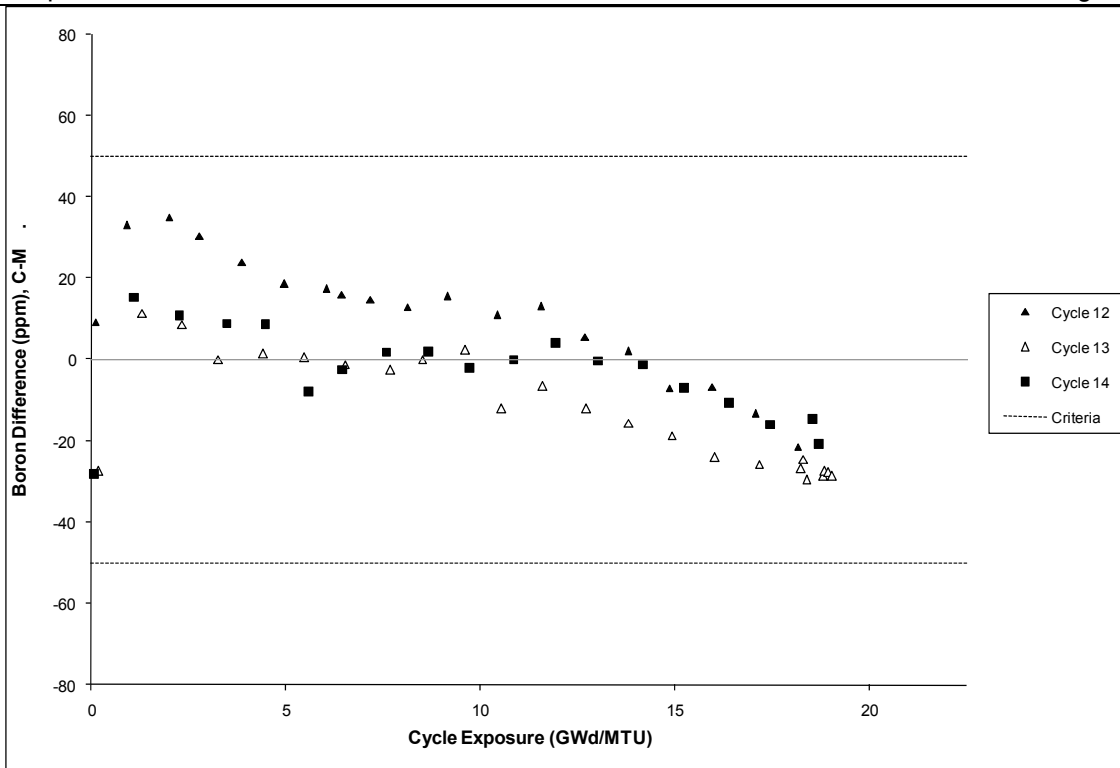


Figure 31-S1-1: Boron Differences

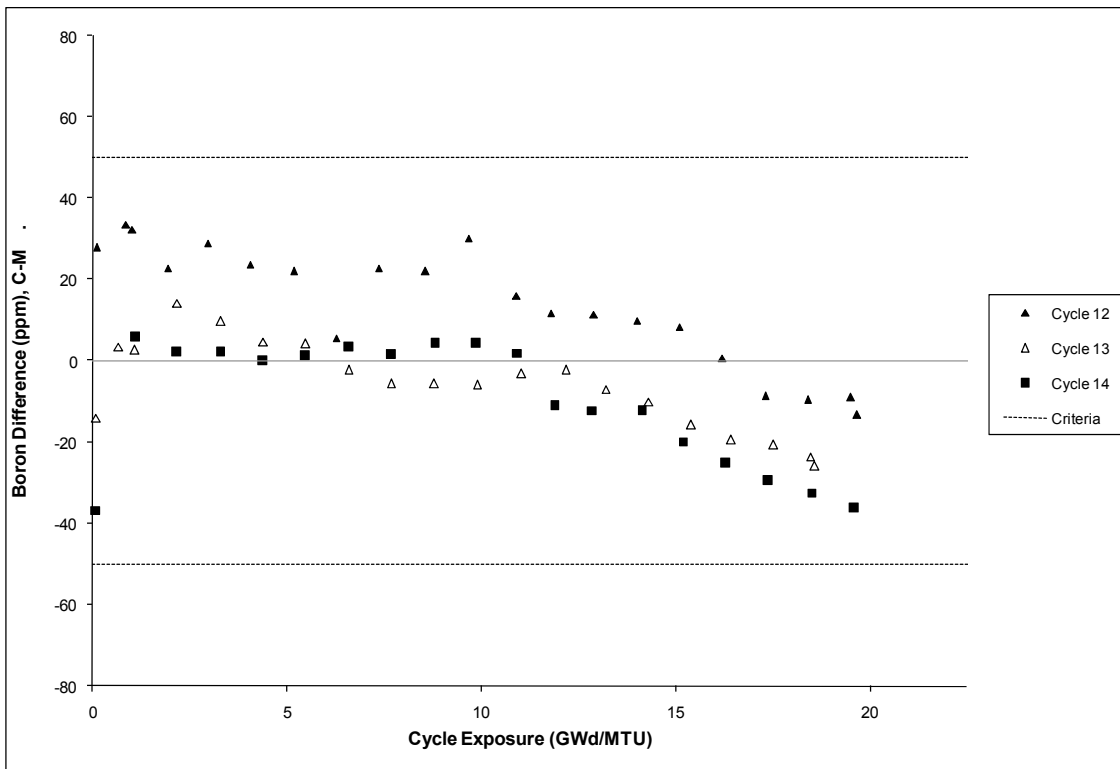


Figure 31-S2-1: Boron Differences

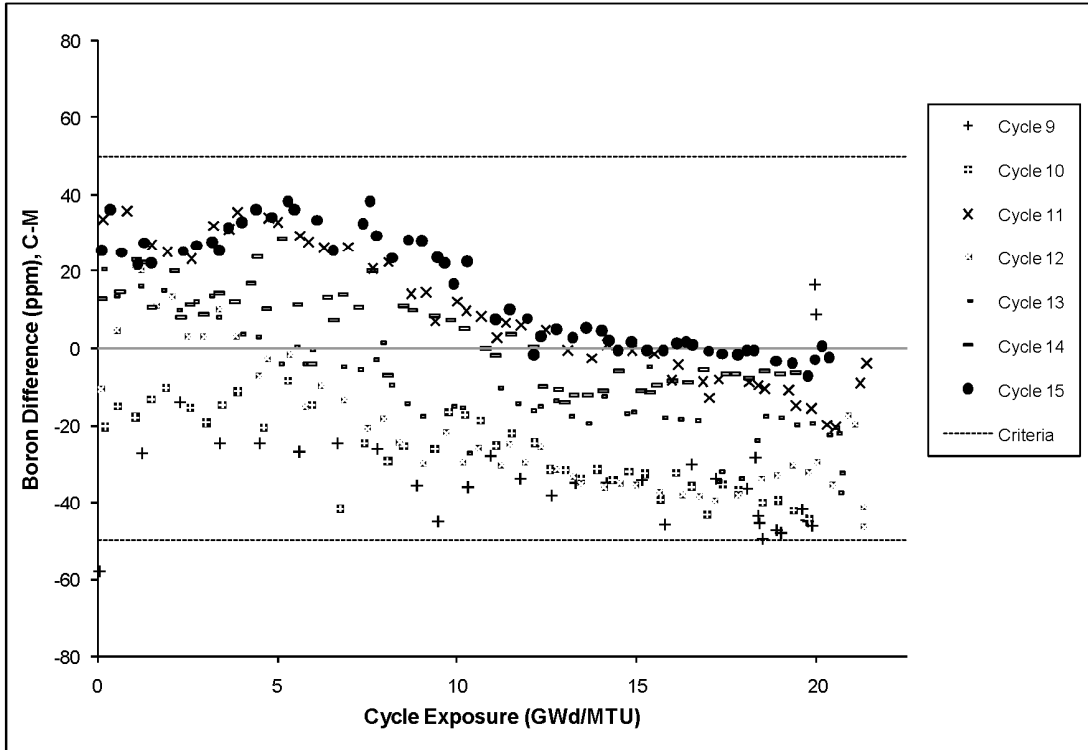


Figure 31-T1-1: Boron Differences

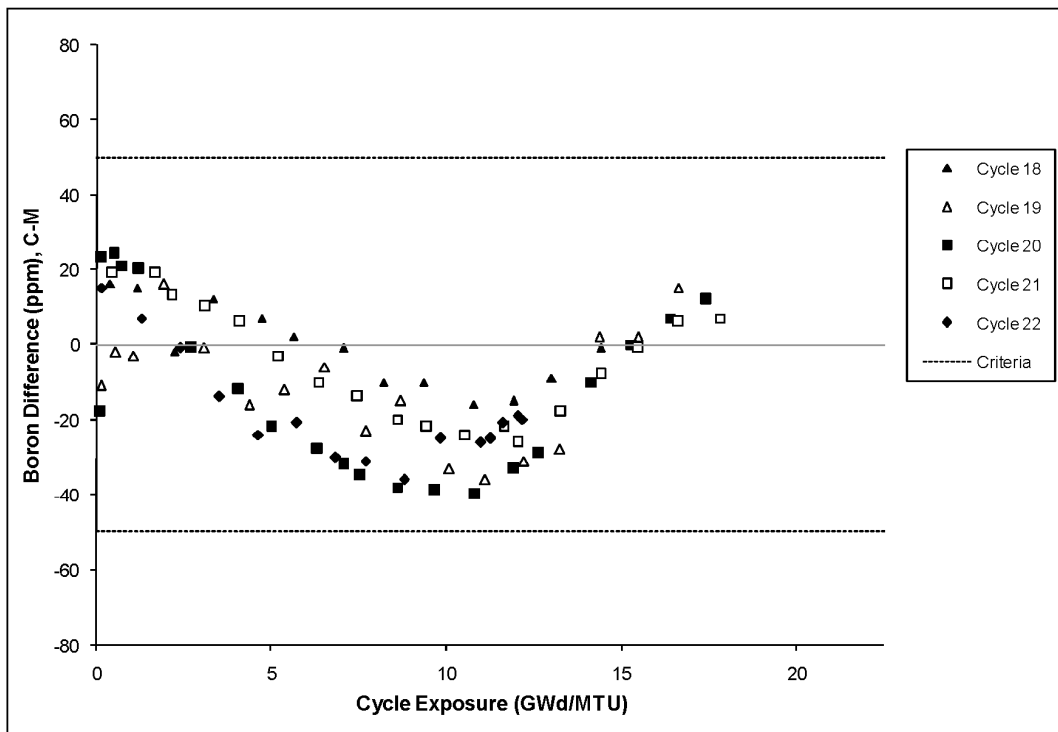


Figure 31-V1-1: Boron Differences

**RAI 32** For the boron comparison cases where the 50 ppm B criteria was not met, a less conservative 500 pcm criteria was selected? Was measured or calculated boron worth used, or predicted differential boron worth? For the cycles with known differences in B- 10 isotopic abundance, was the boron worth used (if predicted) adjusted to account for the different B-10 content? [Page 10-29, 10-30, etc]. if the calculated boron worth is used , justify using the calculated boron worth when the error in the calculated boron concentration exceed the first criteria ?

### AREVA Response

The HZP boron concentration differences (C-M) for Cycles 7 and 8 of Plant A and Cycle 10 of Plant T1 exceed the 50 PPM criterion. No measured boron worths were available for Plant A. Therefore, the respective calculated boron worths were used to make the adjustments for Cycle 7 and 8 of Plant A. A measured boron worth was available for Cycle 10 of Plant T1 and this measured boron worth was used to make the adjustment.

In all cycles of plant A, the measured boron concentrations were adjusted to account for the measured B-10 content. The boron worth calculation is based on the ARTEMIS B-10 content of 19.9 at%. Boron worth measurements are available for some of the benchmark cycles. Therefore, boron worth predictions were made for these cycles and compared to the measured values. Comparisons for plants A, S1 and S2 are shown in the following tables:

Cycle	Measured (pcm/ppm)	Calculated (pcm/ppm)	Difference (C-M) (pcm/ppm)
1	-10.5	-10.43	0.07
2	-8.29	-8.268	0.02
3	-7.67	-7.944	-0.27
4	-7.86	-7.697	0.16
9	-6.42	-6.519	-0.10

**Table 32 -1, Plant A Boron Worth Comparisons**

<b>Cycle</b>	<b>Measured (pcm/ppm)</b>	<b>Calculated (pcm/ppm)</b>	<b>Difference (C-M) (pcm/ppm)</b>
S1, 12	-7.18	-6.93	0.25
S1, 13	-6.88	-6.93	-0.05
S1, 14	-7.04	-6.88	0.16
S2, 12	-7.05	-6.70	0.35
S2, 13	-6.99	-6.72	0.27
S2, 14	-6.92	-6.75	0.17

**Table 32-2, Plant S1 and S2 Boron Worth Comparisons**

These comparisons show good agreement between the predicted and measured boron worths and justify the use of a calculated boron worth to make the adjustment between boron and reactivity.

The response to RAI 28 shows that after the data were properly adjusted for plant G1 that all data met the 50 ppm criterion. Therefore, this question no longer applies to G1.

**RAI 33** For critical boron concentration comparisons, the differential boron worth (DBW) is used to adjust the measured concentration to ARO conditions. It would be prudent to compare measured and predicted boron worths from each cycle's ZPPT, if available. If the predicted boron worth is used to convert the 500 pcm criteria to boron concentration, then the DBW validation may be more important. [Page 10-3]

**AREVA Response:**

See the response to RAI 32.

**RAI 34** Rod worth results may have different uncertainties and biases for different measurement techniques (i.e. rod swap may be more accurate than boron swap). It would be beneficial to provide the rod worth measurement technique with each set of results and attempt to provide a conclusion about the accuracy of the methods vs. each technique. [A-1]

**AREVA Response:**

The table below shows the rod worth measurement technique used for each of the benchmarked plants and cycles. Plants G1 and G2 are not included because bank worth measurement are not performed for these plants.

Cycle	Plant						
	A	B	C	S1	S2	T1	V1
1	Boron Swap	Rod Swap					
2	Rod Swap						
3	Rod Swap						
4	Rod Swap						
5	Rod Swap						
6	Rod Swap						
7	Rod Swap						
8	Rod Swap						
9	Rod Swap					Boron Swap	
10	Rod Swap		Rod Swap			Boron Swap	
11	Rod Swap		Rod Swap			Boron Swap	
12	Rod Swap		Rod Swap	Rod Swap	Rod Swap	Boron Swap	
13	Rod Swap		Rod Swap	Rod Swap	Rod Swap	Boron Swap	
14	Rod Swap		Rod Swap	Rod Swap	Rod Swap	Boron Swap	
15			Rod Swap			Boron Swap	
16			Rod Swap				
17			Rod Swap				
18							Boron Swap
19							Boron Swap
20							Boron Swap
21							Boron Swap
22							Boron Swap

The rod swap measurement technique has been employed by the nuclear industry to help reduce the time required for startup physics testing. The boron swap method has fewer predictions/uncertainties associated with it. The rod swap method has uncertainties associated with the prediction of the reference bank position, the actual measured reference bank position, the test bank position, the measured reference bank worth, and the rod shadowing factors. The boron swap has uncertainties associated with the positions of the individual banks, boron measurements and the shadowing effects of other rods present in the core. However, in the boron swap method it can be difficult to control the dilution and rod pulls to ensure that overshoots or undershoots on reactivity do not occur which can add to the uncertainty of this method.

Since measurements were performed using both techniques, a statistical comparison can be performed. The statistics for the differences in total bank worth  $((C-M)/M*100)$  for the boron swap, rod swap techniques and the combined measurements are provided below:

	Mean (%)	Standard Deviation (%)
Boron Swap		
Rod Swap		
Combined		

The above statistics show that the two measurement techniques used are consistent for the cycles analyzed. The boron swap method does produce a lower standard deviation but has a higher bias. Both methods are statistically within the  $\pm 10\%$  criterion on total rod worth. This is also consistent with the ANSI standard (which uses the same criterion for both rod swap and boron swap).

**RAI 35** For the power uncertainty statistics, the normality of each population of interest should be stated along with the mean and standard deviation. For normal distributions, it is beneficial to also provide the tolerance factors used for the uncertainty calculations. [12-24,12-25]

**AREVA Response:**

The technique does not require normality since the more limiting uncertainty of either a normal or non-parametric uncertainty is used. The frequency distributions are provided to show that the statistical sampling is visually Gaussian (nearly normal) and not too abnormal (no double peaks or large skews). The statistics for the uncertainty calculations are shown in Table 35-1.

**Table 35-1: Uncertainties Assuming Normality\***

	FΔH		FQ
Critical Experiments Mean/Standard Deviation /df	[		
Multi-assembly Mean/Standard Deviation /df			
Core Mean/Standard Deviation /df			
Total Standard Deviation			
Combined Degrees of Freedom			
95/95 K Factor			
Uncertainty (rounded up) Assuming Normality			
		]	

\* Values for mean, standard deviation , and uncertainty are in percent.

**RAI 37** A cumulative standard deviation is provided for the Global Radial Statistics in Table 12.4.1-1, but not for the Global Peak Statistics in Table 12.4.1-2. [Page 12-25]

**AREVA Response:**

As described in the text, the cumulative statistics for this table are not provided because each plant can have a bias relative to the measurement of the grid depressions which does not reflect the calculational accuracy. The text on page 12-13 contains the combined statistics with a mean of [ ] and a standard deviation of [ ] after the bias is removed for each plant.

**RAI 39** *Gadolinia rod power comparison in the multi-assembly calculations with APOLLO2-A and ARTEMIS demonstrate that the agreement gets better as the gadolinium isotopes deplete, but it shows that the uncertainty at 10 GWd/mtU may be as high as the uncertainty at 0.1 GWd/mtU. [Page 12-37]*

**AREVA Response:**

Your observation is correct. The errors look similar to the low burnup case. The peaking in the Gad pins is still below 0.8 power at 10.0 GWd/mtU and the parasitic Gadolinium isotopes are not completely depleted. These cases are being pooled with the low burnup cases and discarded as not limiting. The statistics of the Gad pins for powers less than 0.8 are a mean of [ ] and a standard deviation of [ ] which is slightly worse than the statistics for all pins with powers over 0.8 (mean of [ ] and a standard deviation of [ ]).

**RAI 40** Please provide more detail about how the “grid bias” is calculated and removed from each plant. [Page 12-13]

**AREVA Response:**

The grid bias is seen in many of the Average Axial Power Distribution Figures in the appendix. For those plants with fine axial measurements with grid depressions, the measured result between the grids is generally higher than the calculated result with homogenized grid model. Figure S2 10.47-13 on page S2-15 illustrates this effect for a moveable incore measurement system. In addition, this effect depends upon the grid type and the type of measurement system. In Figure C 10.4.3-55 on page C-62, the measurement system uses fixed incores which are discrete and incapable of measuring the grid depressions. Plants G1 and G2 have an Aeroball system which does not have as fine of an axial resolution as the moveable detectors and the grid depressions are more spread out. Inconel grids with more parasitic properties than Zirconium alloys would have deeper depressions and higher measured peaks than a calculation that homogenizes the grids. For calculational models with homogenized grids, a power peaking bias or uncertainty is applied to account for the grid. As an example, the Inconel grid factor for B&W plants prior to introduction of Zirconium alloy grids was 1.026 multiplier (2.6%) and the Zirc4 grid factor was 1.01 (1%). To estimate the calculational error of a model that is independent of the grid type and measurement system, the bias of the results is removed by multiplying the results by the bias calculated for each plant. These bias adjustments are very close to the grid multipliers for the respective grid type and are a reasonable approach.



**RAI 42** Please provide more details in Figures 12.2.2-1 to 12.2.2-6. What are the units of the values shown? Is it C-M or M-C, for instance? [Page 12-33 to 12-38]

**AREVA Response:**

These are the percent differences between ARTEMIS and APOLLO2  $\{(ARTEMIS - APOLLO2) / ARTEMIS * 100\}$ .

**RAI 43** The error bars on the boron letdown curves appear to be the +/-50 ppm criteria. They are too big to be measurement uncertainty.

**AREVA Response:**

It is correct that the error bars on the boron letdown curves indicate the  $\pm 50$  ppm criterion and not a measurement uncertainty.

**RAI 44** The average axial power shapes of plants C & T appear to be smooth extrapolations of fixed incore detectors. The type of detectors should be provided for each plant, and if the measured axial distribution is calculated from a limited number of fixed signals, the method used for performing the extrapolation should be documented. [Page 10-33]

**AREVA Response:**

The measurement systems used in the benchmarked plants are included in the following table:

Plant	Measurement System
A	Moveable Fission Detector
B	Moveable Fission Detector
C	Fixed Rhodium Detector
G1	Moveable Vanadium Aeroballs
G2	Moveable Vanadium Aeroballs
S1	Moveable Fission Detector
S2	Moveable Fission Detector
T1	Fixed Rhodium Detectors
V1	Moveable Fission Detector

The generation of the “measured axial power shape” from a limited number (N) of axially fixed incore detectors is defined by the following process (Reference [1]):

Predicted (ARTEMIS) power distributions are generated at each axial detector level by axially integrating the predicted axial power distribution over the axial segment of the core corresponding to the detector height. Predicted detector signals are similarly generated at each axial detector level. The ratio of the predicted powers to the predicted signals is used to convert measured signals to measured/inferred powers at each axial detector level.

The above inferred power distribution, corresponding to the N axial detector levels, is expanded into 24 equidistant axial nodes as follows: A predicted 24 equidistant node axial power distribution is generated by axially integrating the predicted axial power distribution over 24 equidistant axial nodes. For each axial detector level, the ratio of the inferred axial power and the calculated axial power is calculated in order to convert the predicted 24 equidistant node axial powers to the measured/inferred 24 equidistant node axial powers.

For equidistant nodes whose centerline lies within a detector span, the ratio from that detector level is used. For nodes below the bottom detector level, the ratio from the bottom detector level is used. For equidistant nodes above the top detector level, the ratio from the top detector level is used. For equidistant nodes whose centerline lies between 2 detector spans, the ratio is determined by linearly interpolating the values from the 2 adjacent detector segments.

---

The 24 equidistant axial node powers in the detected locations is then expanded to the undetected locations in the same manner as used for INPAX-W. The inferred distribution is then renormalized to an average value of 1.0 to produce the final three dimensional nodal power distribution.

### Reference

1. AREVA NP Document, XN-NF-83-01(P), EXXON Nuclear Analysis of Power Distribution Measurement Uncertainty for St. Lucie Unit 1, January 1983

**RAI 45** A summary plot of the difference between calculated and measured axial offset, by cycle, would be beneficial. This may help to discern if the core average axial shape is contributing to the peak assembly power deviations.

**AREVA Response:**

Summary plots showing the calculated to measured AO differences at the points in cycle that are consistent with the core average power maps. This was done so that the measured AO values are consistent with the predicted values. The plots of showing the AO differences are given below:

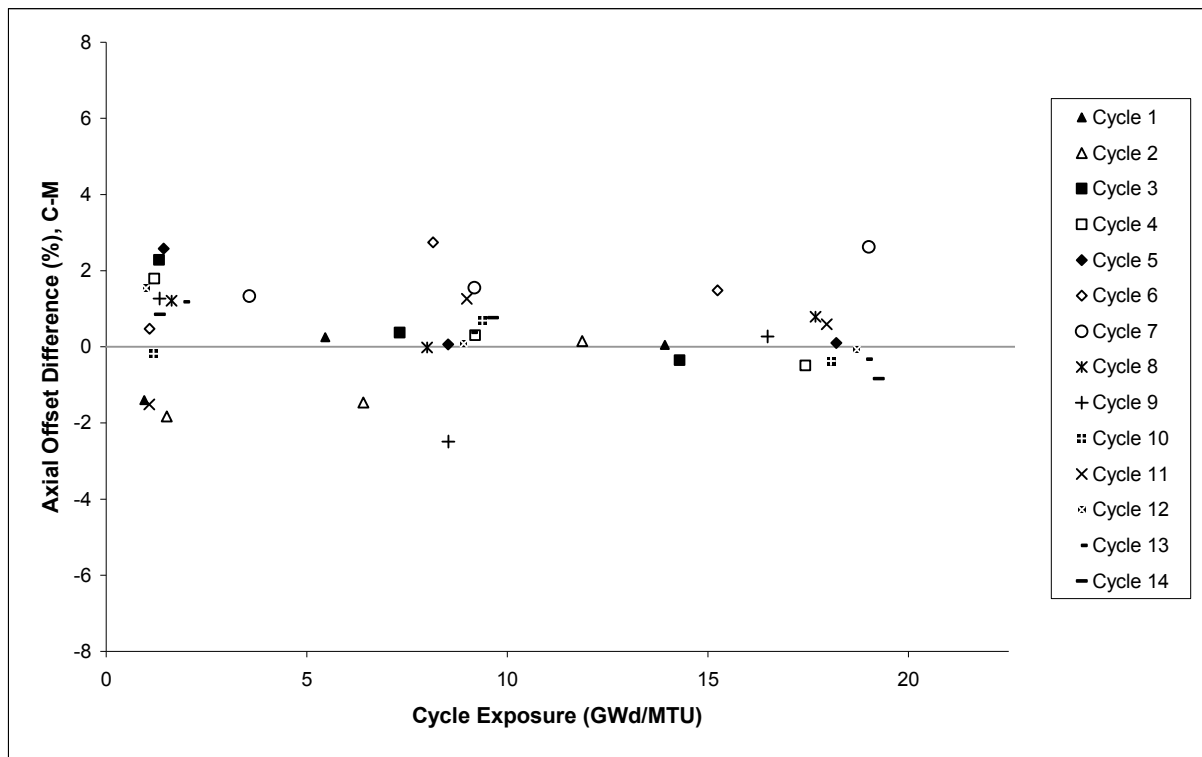


**Figure 45-A-1: AO Comparisons**

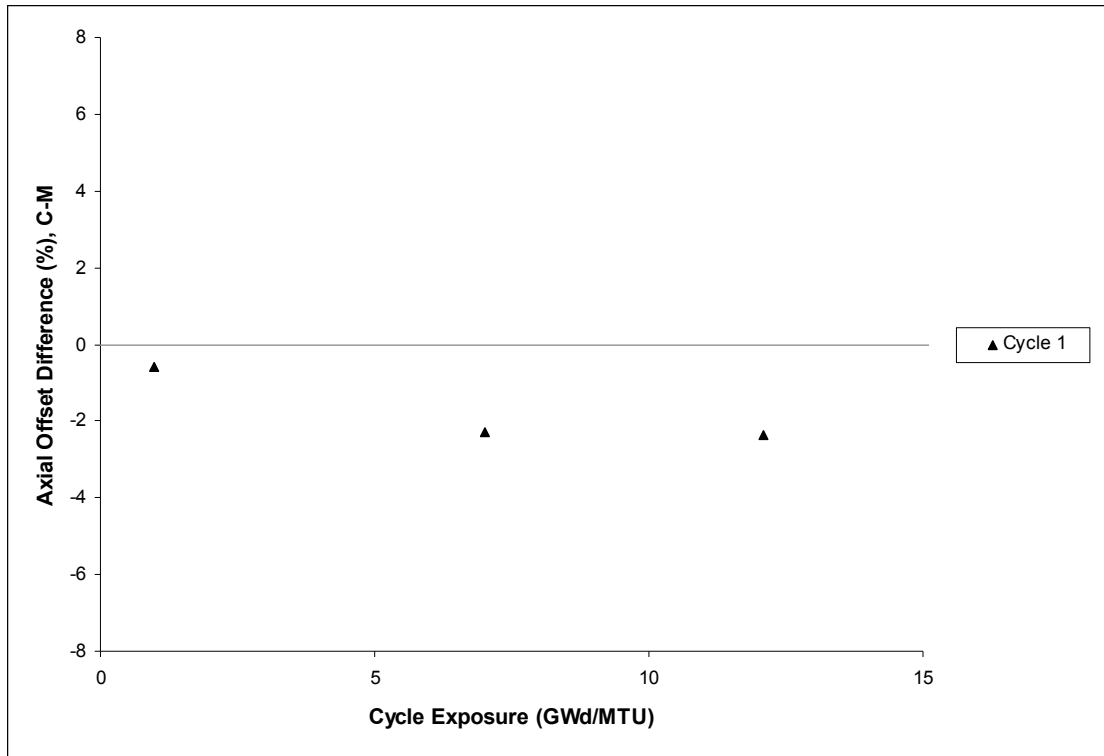


Figure 45-B-1: AO Comparisons

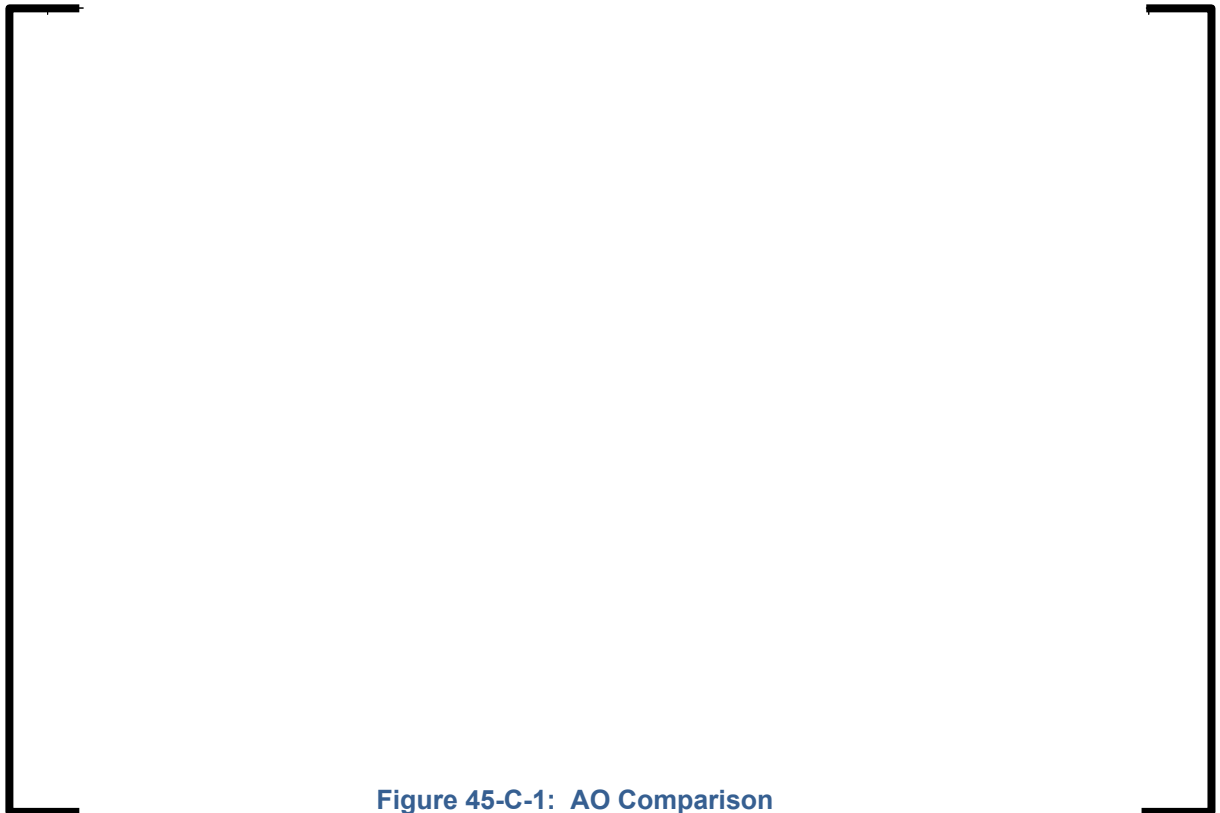


Figure 45-C-1: AO Comparison

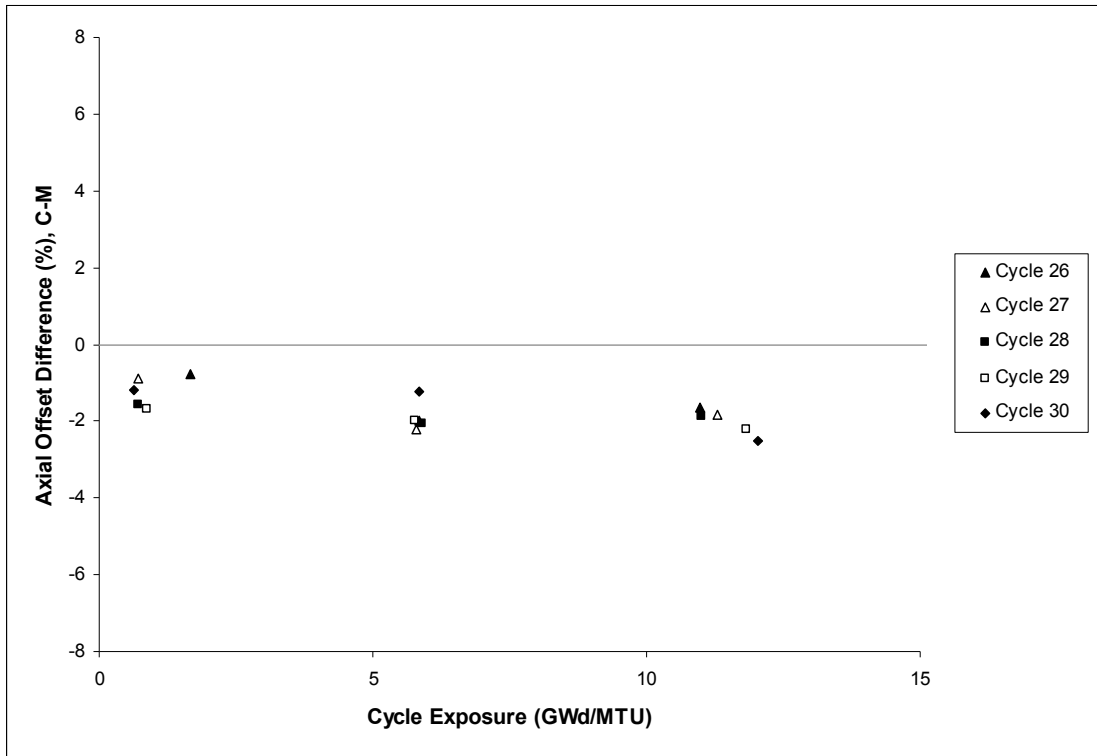


Figure 45-G1-1: AO Comparisons

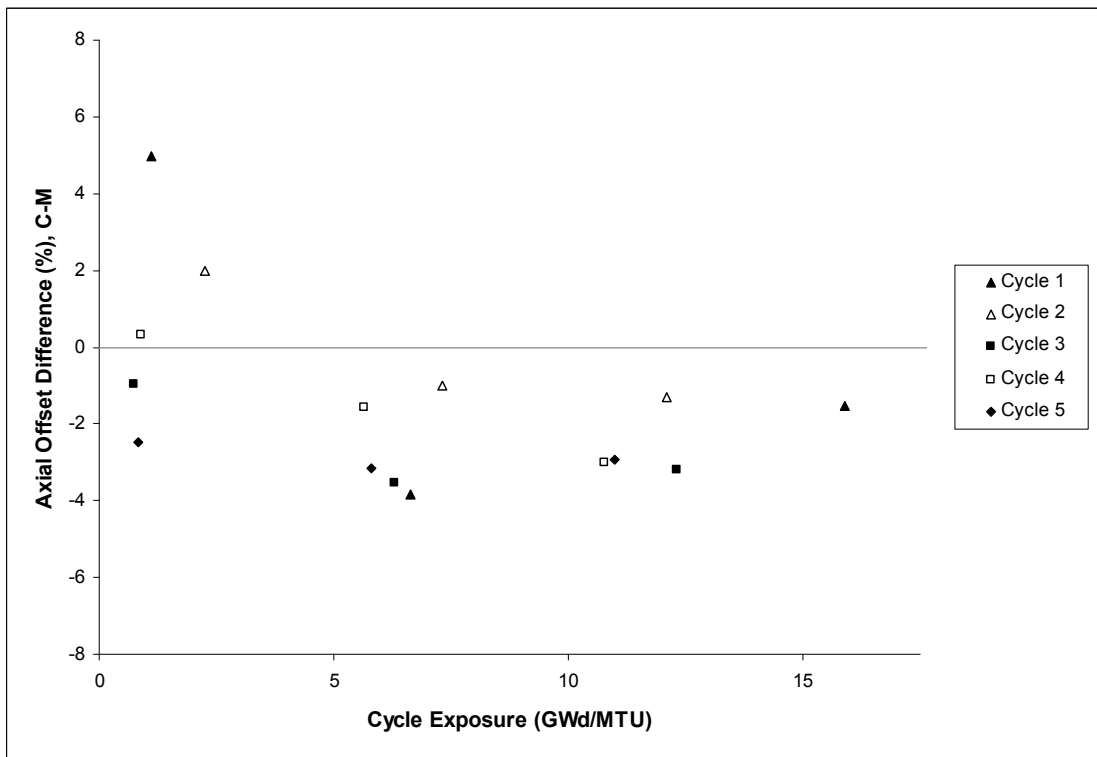


Figure 45-G2-1: AO Comparison

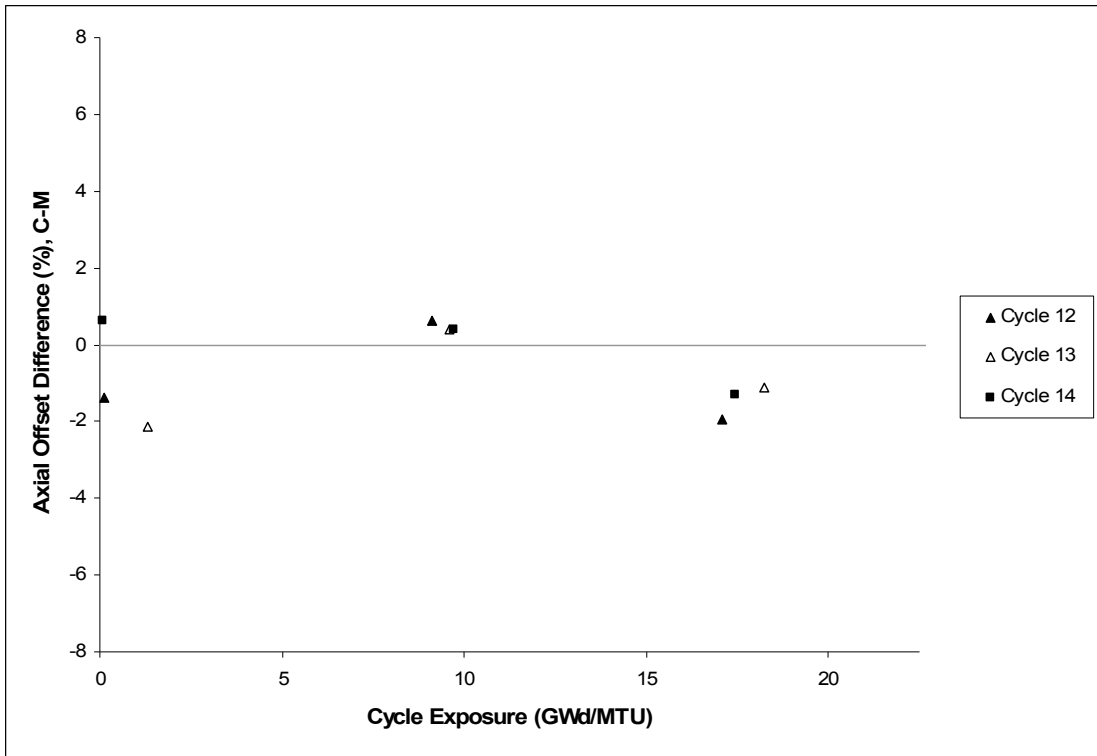


Figure 45-S1-1: AO Comparisons

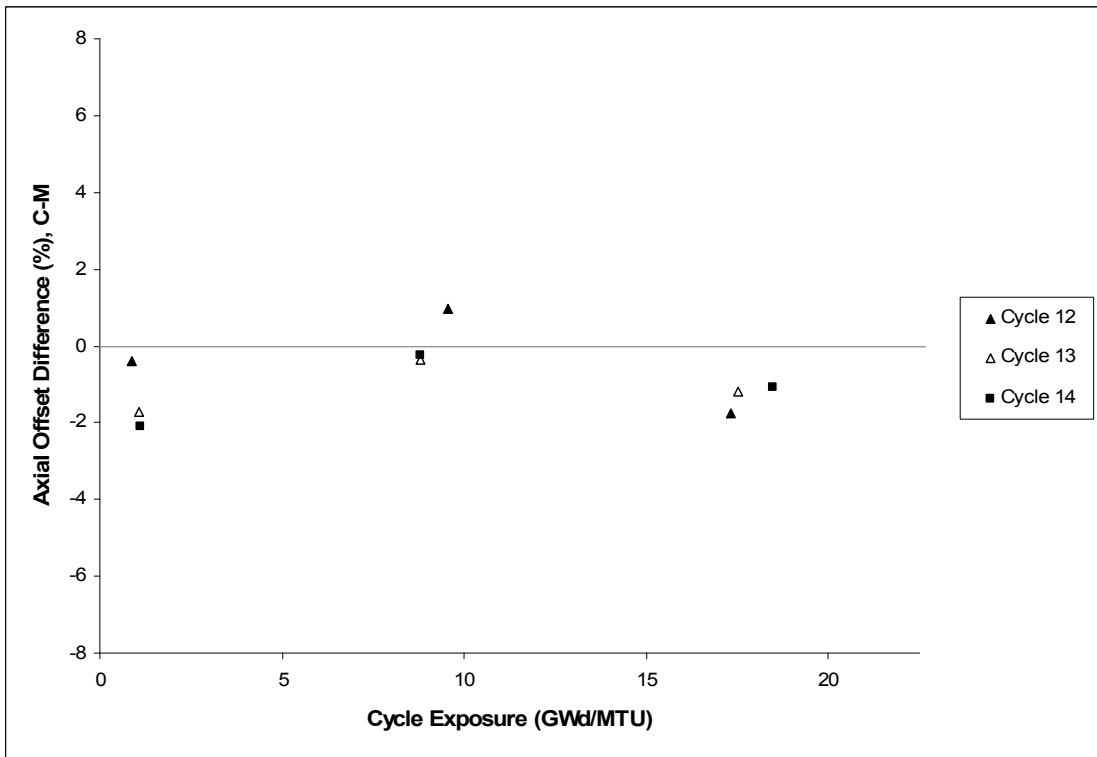
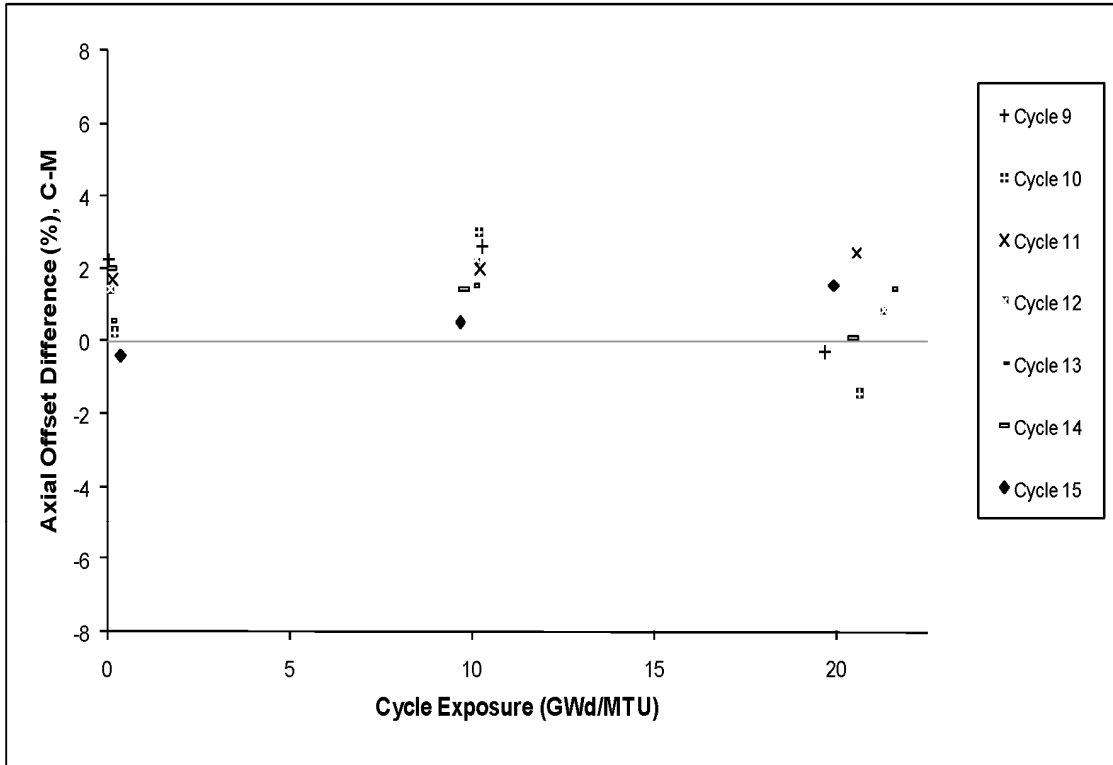


Figure 45-S2-1: AO Comparisons



**RAI 46** *The report states that plant G1 has a 2% bias for the peak assemble power comparison. The context of this statement is the discussion of grid depressions (or lack thereof). However, analysis of the average axial power plots for G1 indicates this deviation is possibly due to an increased difference in core average axial offset and not the lack of compensation of an explicit grid flux depression effect. [Page 12-12]*

**AREVA Response:**

The context of the discussion on Page 12-12 is that the bias for plant G1 is higher than the expected Zr grid bias. The cause of the larger bias was not identified in the topical. The report identified what would be done if a larger bias was found for a plant that implemented these uncertainties with ARCADIA. It states, “The G1 plant does not currently use this uncertainty method but if it did, either the reason for the higher bias would need to be resolved or a higher grid bias would be applied.” From a visual inspection of the core average axial power comparisons, the increased bias above the grid bias in plant G1 could be a difference in axial offset prediction. Any consistent axial offset shift could cause an increase in the bias and would always be super imposed upon the grid bias. On an analytical basis, the “lack of compensation of an explicit grid flux depression effect” should always result in an underprediction of the peak of the magnitudes as stated. In practice, there could be other effects that add or subtract from this grid effect.

**RAI 48** As explained in section 12.1, the inferred uncertainties are based on the ability of ARCADIA to predict the powers in uninstrumented assemblies. Later in section 12.3 the total inferred uncertainties are defined as the sum of the power uncertainty at the uninstrumented assemblies plus the local uncertainties which include the pin power uncertainties from APOLLO2-A and the pin power reconstruction uncertainties from ARTEMIS-APOLLO2-A comparisons. However, it is not clear how the ARCADIA simulation of the plant cycles are used in this process? [Page 12-7]

**AREVA Response:**

References 12.6-1, 12.6-2, and 12.6-6 include detailed descriptions of three different measurement processing systems that include how the core neutronic simulator is used to generate a full core power distribution map from instrumented locations. To perform this calculation, a neutronic core simulator is needed to produce predicted signals, relationships between those signals and power in the assembly for both the measured and unmeasured locations. ARCADIA is used to generate this information for these plants and cycles. In a general sense, the INPAX-W, INPAX-CE, and MEDIAN methods use the calculated power shape to propagate the differences seen between the measured and predicted powers in the measured locations to the unmeasured locations. The global error component of the inferred uncertainty has not been greatly affected by the evolution of core simulators which indicates that the error is dominated by the measurement errors.

**RAI 49** Three measurement systems, INPAX-W, INPAX-CE and MEDIAN AMS, are evaluated for the inferred power distribution uncertainties. The ARCADIA application range statement should mention these systems specifically [Page 13-1].

**AREVA Response:**

The sentence “The three measurement systems evaluated are the INPAX-W system, the INPAX-CE system (also known as INPAX-II), and the MEDIAN AMS.” from page 12-7 does not fully describe the process. There are three types of physical measurement systems, moveable incore, Rh fixed incore, and Aeroball detector systems. Each of these systems uses processing algorithms/software to convert the raw measured data to measured power distributions. The algorithms are the INPAX-W system, the INPAX-CE system (also known as INPAX-II), and the MEDIAN AMS systems, respectively.

The following wording is proposed to be added in the middle of section after the phrase “Framatome designed reactors.” in section 13.1 in the approved version of the topical report.

*These benchmarks include uncertainty verification for plants that use moveable incore, Rh fixed incore, and Aeroball incore detectors.*

The following wording is proposed to replace section 13.3 in the approved version of the topical report.

*AREVA will continue to monitor its methods with respect to current cycle designs for its licensing applications. Prior to licensing a new contract, AREVA will evaluate at least three cycles of data relative to these criteria prior to licensing the first cycle with AREVA fuel with ARCADIA. This includes verification of their measurement uncertainties and/or calculational uncertainties by using the appropriate method presented in Section 12.*

**RAI 50** *Please explain how the FSA component of the uncertainty is calculated in Section 12.3.2 [Page 12-9].*

**AREVA Response:**

The FSA uncertainty component is calculated in a similar manner as the 2D relative power uncertainty component is calculated for the INPAX-W reconstruction methodology. Rather than being the average relative power over the entire length of the fuel (INPAX-W), FSA represents the average relative power over the 4 (for CE reactors) axial heights of the fixed incore detectors.

At each of the 4 axial detector levels, the detector signals are converted to powers and expanded radially to all assembly locations. These 4 x N (# of assy.) powers are then normalized to an average value of 1.0. For a given assembly the FSA term is the average of the 4 normalized values (since all detector lengths are the same). The process to determine the uncertainty of FSA is as described in the first part of Section 12.3. In the 2nd paragraph of Section 12.3, the sentence could read “For a given parameter of interest, e.g. FSA, the methodology...”.

**RAI 51** In section 12.3.2 FR and FZ components of the uncertainty analysis for plant C (INPAX-CE) are calculated using S1, S2 and A plant detector measurements (INPAX-W system). Please justify calculating FR and FZ uncertainties in INPAX-W system and using them in INPAX-CE system [Page 12-9]

**AREVA Response:**

Definitions:

FSA = Average segment power

FR = Ratio of average assembly power to average segment power. The average assembly power is obtained by integrating the power over the entire length of the assembly.

FZ = Ratio of the peak planar power in an assembly to the assembly relative power.

Discussion

The FR and FZ uncertainties represent the ability of the INPAX-CE methodology to reconstruct detailed axial information from the coarse measured information available in the fixed incore detector system. [

]

[

]

**RAI 52** Since the Inconel grids are eliminated from uncertainty analysis due to large grid depressions and only used in the old fuel assemblies, it should be mentioned in the application statement [Page 12-13].

**AREVA Response:**

The qualification of ARCADIA is not impacted by the exclusion of the peak statistics for Inconel grids. Rather, the uncertainty section identifies that grid type and other aspects of plant types could affect the bias of the peak prediction and needs to be addressed for each plant and grid type. This is evidenced by both the Inconel grid discussion and the bias discussion on the G1 plant on page 12-13. The process to define such biases occurs in the implementation phase of the code or fuel contract and could be a simple adjustment of the uncertainty or peaking allowances used in the safety analyses. The following wording is proposed to be added at the end of the replacement for section 13.3 from the response to RAI 49 and included in the approved version of the topical report.

*During the verification of uncertainties, any peaking biases due to grid type or other plant effects will be quantified and accounted for in the uncertainties and/or peaking allowances in the licensing calculations.*

**RAI 54** For multi assembly calculations in Section 12.2.2, provide lattice description (type, enrichment) and lattice combinations used in the 20 multi assembly calculations.

**AREVA Response:**

No response is provided for this RAI. It is expected that this RAI will not be part of the final set of requests.

**RAI 55** Figures 12.2.2-1 through 12.2.2-6 show burnable poison location with no data. Does it mean the relative difference in those pin locations were rejected because of their low power?

**AREVA Response:**

No, these pin locations are guide tube locations filled with rods containing only Al<sub>2</sub>O<sub>3</sub>-B<sub>4</sub>C pellets and have no fission power.

**RAI 61** In Table 12-5.1 Inferred FDH and FQ uncertainties for various power reconstruction methods are compared to the uncertainty criteria. Although it is not clear in the report, based on the references it assumed that these criteria are based on the uncertainties of the previous code systems. Please provide justification for these criteria.

**AREVA Response:**

For the inferred uncertainty verification, the criteria are based on the measurement uncertainty and not on a previous code system. As stated on page 12-6, "Hence, the inferred uncertainty includes the effects of both calculated and measured powers and results in an uncertainty that can be compared to the measurement system uncertainty." The inferred uncertainties are used to estimate the measurement system uncertainty for FΔH and FQ in the specific plant Technical Specifications using AREVA methods. The criteria provided in this Topical are the typical measurement uncertainties encountered for each type of measurement system. Because there can be plant to plant variations of these uncertainties, the process to implement AREVA fuel and methods validates these uncertainties on a plant by plant basis as noted in Section 13.3.

This method has been used by AREVA to validate the application of the INPAX-W, INPAX-CE, MEDIAN, and neutronic core simulators to be used for plant Technical Specification Monitoring. For example, Section 3.3 of the Technical Evaluation Report of the INPAX-W method in Reference 12.6-2 contains the following statement, "It is concluded that the SPC determination of the EMF-93-164(P) uncertainty limits provides a reliable estimate of the INPAX-W calculational uncertainty and is therefore acceptable."

For Nuclear Reliability Factors in Section 12.4 which are not the same error estimates as the inferred errors, the criteria are obtained from a previous code package (Reference 12.6-7) and are currently used in several plants for licensing calculations. Section 12.4 demonstrates that continued use of these uncertainties is conservative for ARCADIA.

**RAI 62** TYPO: Subscripts in Table 6.2-5 are sized inconsistently (Gd3O3). [Page 6-7].

**AREVA Response:**

This issue will be fixed in the approved version of the topical report.

**RAI 63** The transverse-integrated precursor concentration is denoted as  $\xi$  above and below Equation 3-27 instead of  $\zeta$  [Page 3-10]

**AREVA Response:**

This issue will be fixed in the approved version of the topical report.

**RAI 64** Zircaloy is misspelled (as Zircalloy). [Page 6.12]

**AREVA Response:**

This issue will be fixed in the approved version of the topical report.